Sinusoids with linear frequency shift in time series – precise characterisation and removal to support CTBT on-site inspections

Felix Gorschlüter

Kontakt:
Deutsche Stiftung Friedensforschung (DSF)
Am Ledenhof 3-5
D-49074 Osnabrück
Fon: +49 541 60035-42
Fax: +49 541 60079039
www.bundesstiftung-friedensforschung.de
info@bundesstiftung-friedensforschung.de

Felix Gorschlüter
Technische Universität Dortmund
Experimentelle Physik III
Otto-Hahn-Str. 4
44227 Dortmund
Fon: +49 231 755-3520
felix@e3.physik.uni-dortmund.de

Gestaltung, Satz und Herstellung: atelier-raddatz.de und DSF

Spendenkonto der Deutschen Stiftung Friedensforschung:
Sparkasse Osnabrück, DE77 2655 0105 0000 0012 30

ISSN 2193-794X

Contents

Forschung-DSF is published irregularly. The authors alone are responsible for the content of the publications.

Abstract

The aim of this work is to support the Comprehensive Nuclear-Test-Ban Treaty Organization. If the global sensor network raises the suspicion that a nuclear explosion has been conducted or if there is such a suspicion for other reasons, the organisation can be tasked to collect evidence on site. During these on-site inspections, among others, seismic signals are measured to detect aftershocks of the potential underground nuclear explosion which allows the precise localisation of the hypocentre of the event. The area to be investigated can thus strongly be narrowed down, greatly simplifying the taking of gas samples in the soil close to the surface and, if applicable, facilitates the targeted drilling into the explosion cavern.

Since explosions are conducted at great depths and sensors would probably not be placed right above this position, very weak aftershock signals are to be expected. These weak signals are superposed by signals that are produced at or above the surface. Aftershock signals are profoundly non-periodic, whereas many anthropogenic, that is human-made, signals are mostly periodic; especially signals generated by engines are usually highly periodic due to their cyclic way of working. We are developing algorithms that are capable of reducing such disturbances and thus increase the signal-to-noise ratio.

The Fourier transform can distinguish between periodic and non-periodic signals. Periodic signals can be represented by sums of monofrequent sinusoids – their characterisation and removal has been proven to work earlier. This work describes and evaluates a procedure which includes linearly in time changing frequencies, processes a time interval of arbitrary length and provides the noise-reduced data.

An analytic function is introduced for the Hann-windowed discrete spectrum of a sine with linear frequency shift (LFS), defined by the four parameters amplitude, initial phase, initial frequency and frequency-change rate. This function is fitted to the complex values of the magnitude peaks in the given spectrum. If successful, the peaks are removed successively by subtraction of the spectra of LFS sines with the corresponding parameters.

The curve progression of (LFS) sines in the spectral domain reveals parameter dependencies which can be reverted in the sense that characteristics are extracted and utilised to estimate the start parameters for the following fitting.

The success of the characterisation and removal is tested with synthetic (LFS) sines, sometimes superposed on pulse signals or Gaussian white noise i.e. noise with a constant spectral power density. The fit results are quantitatively evaluated by the sum of squared deviations between spectral peak and (LFS) sine. In the case of synthetic signals, where the (LFS) sine parameters are known, the root-mean-square value of the difference between reconstructed and original signal in the time domain gives a measure on the manipulation on the signal by the algorithm.

Then the algorithm is applied to real data. The principal procedure is demonstrated by adding purely synthetic LFS sines to a real seismic event of a coal mine, the resulting peaks in the spectrum are precisely fitted and subtracted resulting in minimal changes between original data and reconstructed ones even if the LFS amplitude is five orders of magnitude stronger than the event.

For real signals, all peaks which have been fitted successfully are reduced to the level of the background, but typically several smaller and sometimes even stronger peaks remain. The acoustic data of a main battle tank are processed successfully in the sense of subtracting most of the strongest peaks. The non-periodic contributions remain in the signal – fitting to the goal of the work. If a peak shape does not match the one of an (LFS) sine, the fit result is not very convincing; thus, strong (pseudo-)periodic components remain in the signal.

In sum, it is possible to reduce the periodic content of time-series data significantly. However, the signals of the vehicles contain non-periodic components which remain in the signal. The achieved reduction of periodic content can increase the signal-to-noise ratio and therefore the chance to detect aftershock signals in data containing periodic disturbances.

Zusammenfassung

Diese Arbeit soll einen Beitrag leisten, um die Organisation des Vertrags über das umfassende Verbot von Nuklearversuchen zu unterstützen. Wurde durch das weltweite Sensornetzwerk ein Verdacht auf die Durchführung einer Kernexplosion ausgelöst oder besteht aus anderen Gründen ein solcher Verdacht, so kann die Organisation beauftragt werden, vor Ort Indizien zu sammeln. Während dieser Vor-Ort-Inspektionen werden unter anderem seismische Signale gemessen, um Nachbeben der potenziellen unterirdischen Kernexplosion zu detektieren, worüber sich der Herd des Bebens präzise lokalisieren lässt. Das zu untersuchende Gebiet kann somit stark eingegrenzt werden, was ein Gasproben-Nehmen zu Analysezwecken im oberflächennahen Boden über dem potenziellen Explosionsort sehr erleichtert und gegebenenfalls das zielgerichtete Bohren in die Explosionskaverne ermöglicht.

Dadurch, dass Explosionen in großen Tiefen durchgeführt werden und die Sensoren wahrscheinlich nicht direkt über diesem Ort aufgebaut würden, ist mit sehr schwachen Nachbebensignalen zu rechnen. Diese schwachen Signale werden überlagert durch andere Signale, die an und über der Erdoberfläche erzeugt werden. Nachbeben sind hochgradig nicht-periodisch, wohingegen viele anthropogene, also vom Menschen gemachte, Signale überwiegend periodisch sind; insbesondere die von Motoren erzeugten Signale sind durch die zyklische Arbeitsweise für gewöhnlich hochgradig periodisch. Wir entwickeln Algorithmen, die solche Störungen reduzieren können und damit das Signal-Rausch-Verhältnis verbessern.

Die Fouriertransformation kann zwischen periodischen und nicht-periodischen Signalen unterscheiden. Periodische Signale können durch Summen monofrequenter Sinusse dargestellt werden – sie zu charakterisieren und zu entfernen wurde bereits gezeigt. Diese Arbeit beschreibt und bewertet eine Prozedur, die Frequenzen, die sich linear mit der Zeit ändern, einschließt, ein Zeitintervall beliebiger Länge bearbeitet und die Störungs-reduzierten Daten liefert.

Eine analytische Funktion wird eingeführt für das diskrete Spektrum eines Sinus mit linearer Frequenzänderung (LFS – englisch: linear frequency shift) und mit Hann-Fensterfunktion, definiert durch die vier Parameter Amplitude, Anfangsphase, Anfangsfrequenz und Frequenzänderungsrate. Diese Funktion wird an die komplexen Werte der Betragsspitzen im gegebenen Spektrum angepasst. Bei Erfolg werden diese Spitzen nacheinander durch Subtraktion der Spektren von LFS-Sinussen mit den entsprechenden Parametern entfernt.

Der Kurvenverlauf von (LFS-)Sinussen im Spektralbereich enthüllt Parameterabhängigkeiten, die invertiert werden können in dem Sinne, dass Eigenschaften extrahiert und verwendet werden, um Anfangswerte für die anschließende Anpassung zu schätzen.

Der Erfolg dieser Charakterisierung und Entfernung wird mittels synthetischer (LFS-)Sinusse geprüft – manchmal gepulsten Signalen überlagert oder Gauß'schem weißen Rauschen, d.h. einem Rauschen, dessen Leistungsdichtespektrum konstant ist. Die Anpassungsergebnisse werden durch die Summe der quadrierten Abweichungen zwischen der spektralen Spitze und dem (LFS-)Sinus quantitativ ausgewertet. Im Falle von synthetischen Signalen, bei denen die (LFS-)Sinusparameter bekannt sind, gibt der Effektivwert der Differenz zwischen rekonstruiertem und Originalsignal im Zeitbereich ein Maß für die Manipulation des Signals durch den Algorithmus.

Dann wird der Algorithmus auf reale Daten angewendet. Das prinzipielle Vorgehen wird demonstriert durch die Addition von rein synthetischen LFS-Sinussen zu einem realen Ereignis von einem Kohlenbergwerk: Die sich ergebenden Spitzen im Spektrum werden präzise angepasst und subtrahiert, was minimale Änderungen zwischen Original- und rekonstruiertem Signal erzeugt, selbst wenn die LFS-Amplitude fünf Größenordnungen stärker ist als das Ereignis.

Bei realen Signalen werden alle Spitzen, die erfolgreich angepasst wurden, auf das Niveau des Untergrunds reduziert, aber für gewöhnlich bleiben dabei einige kleinere und manchmal sogar stärkere Spitzen erhalten. Die akustischen Daten eines Kampfpanzers werden in dem Sinne erfolgreich verarbeitet, dass die meisten der stärksten Spitzen subtrahiert werden. Die nicht-periodischen Beiträge bleiben im Signal, was dem Ziel der Arbeit entspricht. Wenn die Form einer Spitze nicht zu der eines (LFS-)Sinusses passt, ist das Anpassungsergebnis nicht sehr überzeugend – somit bleiben starke (pseudo-)periodische Komponenten im Signal erhalten.

Insgesamt ist es möglich, den periodischen Inhalt in Zeitreihendaten erheblich zu reduzieren. Die Signale von Fahrzeugen enthalten jedoch nicht-periodische Komponenten, die im Signal verbleiben. Die erreichte Verringerung von periodischem Inhalt kann das Signal-Rausch-Verhältnis und somit die Wahrscheinlichkeit erhöhen, Nachbebensignale in Daten, die periodische Störungen enthalten, zu detektieren.

1 Introduction

I Motivation

Nuclear weapons are a strong instrument to provoke other states or deter them from threatening the possessing state. But there is the security dilemma: having nuclear weapons might be an advantage for the possessing state but if multiple states possess them, the security is reduced for all because of the disastrous impact of these weapons should a possessing country be assaulted and revert to their launch. To keep the number of nuclear weapon states limited and prepare nuclear disarmament, an international agreement stipulates a stop of the spread of nuclear weapon technology around the globe and even the obligation to negotiate about disarmament of the existing weapons (Treaty on the Non-Proliferation of Nuclear Weapons, 1970). To prevent further weapon development the Comprehensive Nuclear-Test-Ban Treaty was concluded in 1996.

1 Types of nuclear weapons

The first nuclear weapons used nuclear fission. The next step in qualitative development were fusion (hydrogen) bombs. At all times these thermonuclear weapons have been two-staged: At first a fission process – which is similar to the explosion of a fission bomb – is used to ignite the second stage of a nuclear fusion. Consequently, without being able to produce a fission bomb, fusion bombs are not feasible. The fission material in the nuclear warhead has to have low concentrations of isotopes which either absorb neutrons without producing new ones or have a too high decay activity which could lead to premature ignition. These essential prerequisites, combined with further conditions[1], greatly reduce the number of suitable materials for the fission stage of nuclear warheads.

Nuclear tests cannot be scaled arbitrarily due to the underlying chain reaction principle. The total fissionable mass is limited because the explosion drives it away before it can be hit by neutrons produced by unpreventable spontaneous fission.[2] Downscaling is challenging because of the exponential energy release with the number of generations before the material is dispersed. The decision on the order of magnitude, with which energy is released during the reaction, lies in the kinetics of the last few fission generations. This makes it extremely difficult to reduce the total energy release by certain factors. A reduction of the mass of fission material close to the critical mass (which is the absolute lowest limit) bears the probability that the energy release is insignificant and the bomb fails as such.

From this it follows that a successful explosion is always accompanied by a minimum amount of nuclear fission reactions, with the production of a minimum of fission products and a minimum of energy release. These products and secondary products can be used to detect nuclear explosions reliably.[3]

2 The Comprehensive Nuclear-Test-Ban Treaty Organization

Either the extensive enrichment of uranium or the test explosions that are necessary at least for the implosion bomb design can be used for detection of states on their way to nuclear weapons. Since decades international treaties are the means to control testing and non-proliferation; one of them is the Partial

1 A minimum cross section of fast neutron induced fission, availability or producibility, manageability like reactivity, storage properties etc.

2 Thermonuclear weapons can be upscaled arbitrarily because the materials used for the fusion of nuclei can be stored densely without a chance of self-ignition of a chain reaction.

3 E.g. the energy release causes high pressures which under ground will create a cavity and excite seismic, acoustic or – in water – hydro-acoustic waves. Additionally, radionuclides transported by wind may be detected. These are not only released from above-ground nuclear explosions but also from underground tests deeply buried – diffusion and barometric pumping often bring isotopes (especially noble gases) to the surface. Once released to the atmosphere, few atoms can be enough to indicate a nuclear explosion [1].

Nuclear Test Ban Treaty (PTBT)[4] from 1963, restricting nuclear explosions to underground ones. It was adopted mainly to stop the release of fallout responsible for a significant increase of radiation all over the world. The treaty still allowed underground tests meaning that the advancement of the weapons could continue. For a comprehensive test ban methods and instruments of verification were required because of fears of strong strategic disadvantages if testing would continue clandestinely for one party. It is insufficient to only detect seismic events, but – because of hundreds of small natural earthquakes every day – one must discriminate between earthquakes and explosions. Scientists developed convincing procedures[5] to automatically reject most of the natural events and in 1996, after years of intensive efforts, the multilateral Comprehensive Nuclear-Test-Ban Treaty (CTBT) was adopted by the United Nations General Assembly [3]. Since then the Comprehensive Nuclear-Test-Ban Treaty Organization (CTBTO),[6] among other things, builds up and maintains the International Monitoring System IMS to ensure that no successful nuclear test is conducted undetected.[7]

The most reliable evidence that an atomic fission took place is the detection of certain radio isotopes or even ratios of isotope concentrations that can be assigned to a small geographical area of release. The strongest challenges are underground tests; the main method is to detect the explosion via seismic sensors at large distances. Typically multiple measurement stations with multiple sensors each allow the localisation of the source mostly by onset times with an accuracy of 10-20 km on the whole globe [6]. To investigate uncertainties, e.g. after a state had announced a strong conventional explosion, an OSI can be conducted in the case of initial suspicion to collect further indications. Using the seismic data of the IMS to locate the origin of the signal results in an error ellipse containing an area up to $1,000\,\mathrm{km}^2$ which is too large to cover it completely with isotope sampling. Several techniques are developed to further reduce this area [7], [8]. The most developed one is to set up local arrays of seismic sensors at the surface in the area of interest (up to $1,000\,\mathrm{km}^2$, Protocol to the CTBT: II.A.3) and to detect and locate aftershock signals coming from the cavity and its vicinity.[8] The problem here is that the signals are weak – for example they can stem from rocks falling 50 m until they hit the bottom of the cavity or from relaxation cracks in the surrounding material – and need to propagate 1 km or more through (different layers of) soil up to the surface where they are to be measured. Because of their low amplitudes, these signals are very susceptible to disturbances which can be either anthropogenic or natural. The former is produced by traffic, construction sites, the mining industry or the like and could even be produced intentionally to mask the signals to hide the test. Furthermore the inspectors themselves produce noise with vehicles and helicopters during measurements and maintenance of their sensors. During the planning of the placement of the seismic sensors, attention is paid to the surrounding noise sources to prevent disturbances in advance, but some disturbances will always reduce the signal-to-noise ratio (SNR) of the data. The reduction of disturbances which have already been measured is the motivation of this work.[9]

3 Periodic and broadband signals

The Fourier transform gives the spectrum of a given interval of time-domain data [13]. Periodic signals are superpositions of sine waves in which every sine shows up as a peak in the spectrum at the frequency of the sine. Non-periodic signals have a broadband spectrum. Therefore these two classes of signals can

4 Treaty Banning Nuclear Weapon Tests in the Atmosphere, in Outer Space and Under Water. It was signed and ratified by the governments of the Soviet Union, the United Kingdom and the United States which was the condition for the entry into force on October 10, 1963. Additionally many more states ratified or acceded to the treaty.

5 "[...] comparison of teleseismic body-wave and surface-wave amplitudes has empirically been shown to provide an excellent discriminant. Surface waves from a shallow earthquake with the same body-wave strength as an explosion are typically 6 to 8 times larger than surface waves from the explosion" [2].

6 To be accurate it is the Preparatory Commission for the CTBTO – the Treaty did not yet enter into force since the ratifications by China, Egypt, India, Iran, Israel, North Korea, Pakistan and the United States are still pending [4]. Nonetheless, the Treaty already has 183 members (May 2014) and the preparation of the International Monitoring System (IMS) is almost complete. The IMS measures non-stop and exercises for on-site inspections (OSIs) are held.

7 The prescribed detection threshold is 1 kt TNT equivalent anywhere on Earth. Actually it is around 0.1 kt for most areas [5]. It is very elaborate if not impossible to plan a nuclear explosion on a smaller scale especially for newcomers.

8 In solid ground a nuclear explosion will always form a cavity because of the high pressure being the product of the extremely high energy release. It can vary in size and stability. Typical diameters are roughly in the order of 60 m [9] (the diameter increases with the the cubic root of the yield [10]).

9 Parallel research in the group Physics and Disarmament asks whether acoustic damping around the seismic sensors can reduce acoustic-seismic coupling [11, 12].

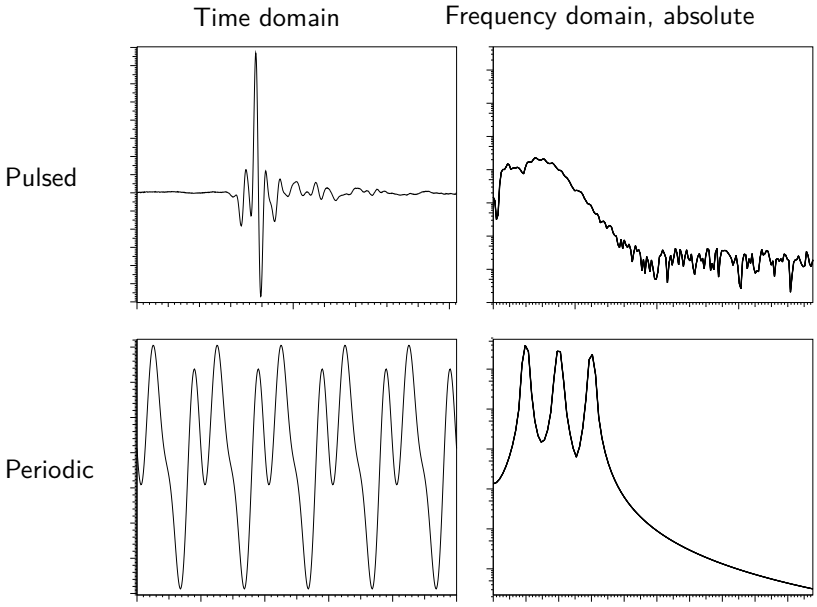

Figure 1.1.: Examples for periodic and broadband signals: The pulsed signal stems from a firecracker (seismic); the periodic one is synthetic, to see the periodicity easily, its frequencies are chosen to be integer multiples of each other so they produce the same form for each period of the fundamental frequency in the time domain. Labels for the axes are omitted in order to focus the attention on the curve shapes.

be distinguished from each other in the spectral domain. Examples are shown in Figure 1.1. Many anthropogenic signals are mostly periodic: Combustion engines run in cycles whereby periodic vibrations occur by the ignition of the fuel-gas mixture at a certain rate as well as periodic emissions of fumes at the exhaust opening. Especially the latter produces acoustic excitations which is of interest because acoustic signals couple to the ground [11]. Consequently even aircraft signals are measured with seismic sensors buried near-surface. Rotors have a certain revolution rate; they cut through the air and return to the same location after one revolution.[10] The acoustic waves of helicopters and propeller aircraft in general produce periodic seismic signals which are commonly measurable with near-surface velocity or acceleration sensors even in hundreds of meters distance to the source.

4 Time-varying frequency

A pure sine is a special kind of time-dependent signal. It has a constant amplitude, and a phase angle that varies linearly in time. The time course of this phase angle implies the frequency (the rate of phase change) and the start phase. If a sine changes its frequency sufficiently slowly certain properties of the sine remain in part; for example it still can be distinguished from non-periodic signals in the spectral domain. Main fields for the occurrence of time-shifting sines are changes in revolution rates of engines or the change of Doppler shift of moving engines. Figure 1.2 shows an example for each. After constant frequency, the next complexer order of a change to the phase angle is a linear frequency change, that is a quadratic increase of phase with time.

5 About this work

The analysis and subtraction of both the monofrequent sine and the sines with a linear frequency shift are introduced, described and evaluated in detail in my doctoral dissertation [14]. This report gives an

10 Multi-blade rotors produce frequencies of multiples of their revolution rate (because of their superposable rotation symmetry), then typically the n-th harmonic is the strongest if n is the number of blades. Another reason for the occurrence of harmonics is that the excitation usually is not sinusoidal.

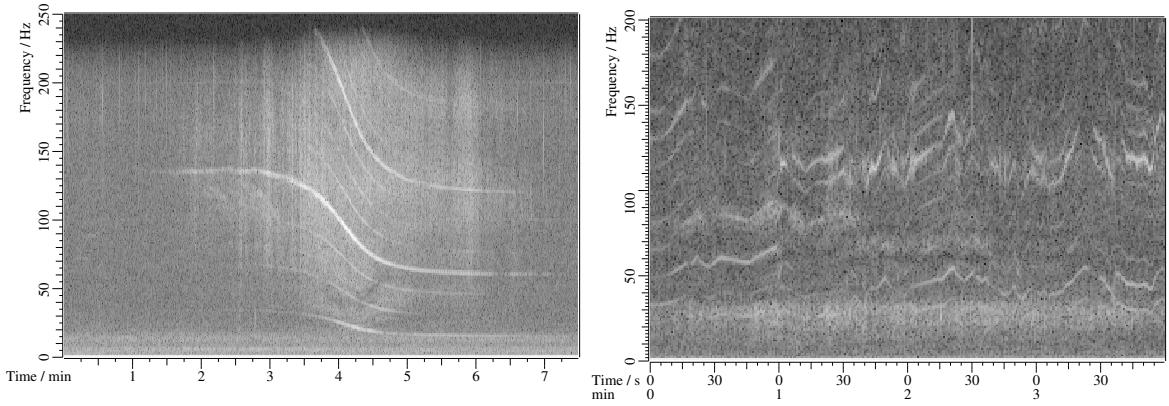

Figure 1.2.: Sequences of spectra (spectrogram, that is time-frequency representation) to demonstrate changes in periodic signals. The grey scale is logarithmic and proportional to the spectral power – the brighter the stronger the spectral power. Vertically limited narrow bright regions indicate periodicity at these frequencies; persistent in time, they form horizontal lines. If frequencies change in time, lines are aslant. If a source does not produce perfect sinusoids, harmonics appear, keeping the same relative distance to each other. Left: a propeller aircraft flying towards the sensor, reaching the point of closest approach at approximately 4 min, then the distance increases again so that the frequencies at the sensor appear to be lower. Right: a land vehicle; it is easy to recognise fast changes in the revolution rate of the engine.

overview of the work. The algorithm design and the mathematical expression for the monofrequent sine have been developed before by Jürgen Altmann [15] and during my Diploma thesis [16].

II General usability

The support of OSIs of the CTBTO is only one application. In this work a general method is analysed to improve time-series data in terms of periodic disturbances. For this purpose mathematical expressions are derived allowing a fit routine to precisely determine the parameters representing the disturbances and allowing their subtraction from the data. That is why in Chapter 4 (real-data analysis) for some events seismic data are processed, for others acoustic ones; acoustic data can have some advantages like easier producibility, better SNR or – in older measurements – a higher sampling rate.

2 Theory

I Introduction

In order to reduce the (quasi-) periodic content in time-series data, sine waves, potentially with linear-frequency-shift (LFS), are to be subtracted from the signal if their parameters are known. Because every sine component produces a single peak in the spectrum, this is to be done one by one. The knowledge of the parameters of a single sine is to be gained by fitting them to its peak in the spectral domain. Our typical approach is to use a fitting algorithm that fits the continuous, theoretical function to the data with the help of its derivatives with respect to the parameters. In this work the Levenberg-Marquardt algorithm is used and the theoretical function and its first derivatives are developed in this chapter.

Beside the sine function itself, three facts need to be taken into account to calculate the expression for the fit algorithm: [13]

- Real data are gained by analogue-digital converters (ADCs) by sampling the continuous signal with a certain rate;[11] thus the data consist of a sequence of equidistant discrete values. This is represented mathematically by multiplying the continuous sine function with an equidistant Dirac comb.
- Real signals can only be handled for a finite duration. In addition they can change over time, whereas the (continuous) Fourier spectrum has no time resolution. Short-term signals in a long interval of data being transformed will therefore be suppressed, which is a reason to limit the interval durations to small ones. Mathematically this means multiplication with a rectangle function. For real data, the interval will consist of 2^n ($n \in \mathbb{N}$) samples in order to apply the fast Fourier transform (FFT) [17].
- Because of the first two items mentioned the discrete spectrum of a monofrequent sine does not necessarily consist of two δ functions at the frequency of the sine and its negative (as would hold for the Fourier transform of the continuous, monofrequent sine) but depends on the difference between the frequency of the sine and the closest frequency of the Dirac comb in the spectral domain. The bigger this difference is, the bigger the effect called "spectral leakage" will be. In order to reduce the effect that small changes of the frequency of the sine have a strong influence on the shape of the peak in the spectrum, window functions are used [18]. Here we use the Hann window by multiplying each interval of data with the corresponding window function before performing the FFT.

1 The Levenberg-Marquardt algorithm

The Levenberg-Marquardt fit algorithm changes the parameter vector of a continuous function along its gradient to find a minimum in the sum of squared deviations between input values and function values at the same positions. Strictly speaking, it minimises:

$$\chi^2 = \sum_{i=0}^{n_{\mathsf{Fit}}-1} \frac{(a_i - \mathsf{f}_a(i))^2}{(\mathsf{w}(i))^2}, \tag{2.1}$$

where:

- n_{Fit} is the number of (complex) values used.
- a_i is the i-th discrete value of the input.

11 For instance, the CTBTO samples with 500 Hz when performing on-site inspection exercises. In all measurements we performed ourselves during the last years we sampled with 10 kHz. Firstly, because we are interested also in higher frequencies. Secondly, as we usually include microphones, one could listen to the recorded data and even understand human speech.

- $\mathsf{f}_a(i)$ is the value of the continuous function, calculated for the current set of parameters and evaluated at the same position as the i-th discrete value.
- $\mathsf{w}(i)$ is a weight for the difference produced by the i-th value, here taken as constant.

Since this measure sums up positive terms exclusively, it tends to increase linearly with n_{Fit}. It is reasonable to normalise it in order to get comparable values with respect to different peak widths: $\chi^2_n = \chi^2/n_{\mathsf{Fit}}$.

II Components required for the theoretical function

Four components are required in order to derive the expression needed for the fit algorithm: (LFS) sine, rectangle, Hann window and Dirac comb. The following parameters are used:

t : continuous time,

ν : continuous frequency,

T : duration of the time interval for one spectrum,

N : number of discrete samples used for one spectrum,

Δt : time between two samples in a discrete time series (resolution in the time domain),

$\Delta\nu$: interval between two neighbouring discrete frequencies (resolution in the frequency domain).

A_0 : amplitude of an (LFS) sine function,

b_0 : LFS parameter of a an LFS sine function,

ν_0 : (initial) frequency of an (LFS) sine function,

ϕ_0 : initial phase of an (LFS) sine function,

where: $T = N \cdot \Delta t$ and $\Delta\nu = {}^1\!/_T$.

1 The continuous and discrete Fourier transform

The continuous Fourier transform is defined as [13, Chap. 2.1]:

$$\mathsf{x}(t) \circ\!\!-\!\!- \mathsf{X}(\nu) = \int_{-\infty}^{\infty} \mathsf{x}(t)\, \mathrm{e}^{-\mathrm{i}2\pi\nu t}\, \mathrm{d}t. \tag{2.2}$$

The discrete Fourier transform of a sequence x_n is defined as [13, Chap. 6.2]:

$$X_k = \sum_{n=0}^{N-1} x_n \mathrm{e}^{-\mathrm{i}2\pi kn/N}. \tag{2.3}$$

2 LFS sine

Each such sine has an amplitude A_0, an initial frequency ν_0, an LFS parameter b_0 and a initial phase ϕ_0, its continuous time course is:

$$\hat{\mathsf{s}}(A_0, b_0, \nu_0, \phi_0, t) = A_0 \sin\left(2\pi\left(\frac{b_0}{2}\cdot t + \nu_0\right)\cdot t + \phi_0\right), \tag{2.4}$$

and the corresponding continuous spectrum:

$$\hat{\mathsf{S}}(A_0, b_0, \nu_0, \phi_0, \nu) = \frac{A_0}{2}\sqrt{\frac{1}{2b_0}}\,(1+\mathrm{i})\left(\mathrm{e}^{\mathrm{i}\frac{\pi(\nu_0+\nu)^2}{b_0}-\mathrm{i}\phi_0} - \mathrm{i}\mathrm{e}^{-\mathrm{i}\frac{\pi(\nu_0-\nu)^2}{b_0}+\mathrm{i}\phi_0}\right). \tag{2.5}$$

3 Rectangle function

Let $\mathsf{r}(t)$ be the rectangle function from 0 to T, then the Fourier transform can be gained directly by execution of the integration:

$$\mathsf{r}(t) = \Pi\left(\frac{t}{T} - \frac{1}{2}\right) \circ\!\!-\!\!- \mathsf{R}(\nu) = \frac{1}{\mathrm{i}2\pi\nu}\left(1 - \mathrm{e}^{-\mathrm{i}2\pi\nu T}\right) \tag{2.6}$$

4 Hann window function

The Hann window function consists of one period of a (co-)sine shifted in a way that it becomes zero at its margins. The continuous Fourier transform can be deduced from the transformation of a general sine (Sec. 2) as the cosine is a phase shifted sine and the Fourier integral of a constant is the delta function at frequency zero.

$$\mathsf{h}(t) = \frac{1}{2} - \frac{1}{2}\cos\left(\frac{2\pi t}{T}\right) \circ\!\!-\!\!- \mathsf{H}(\nu) = \frac{1}{2}\delta(\nu) - \frac{1}{4}\delta(\nu+\Delta\nu) - \frac{1}{4}\delta(\nu-\Delta\nu) \tag{2.7}$$

5 Dirac comb

Sampling with a certain frequency means that every Δt one sample is taken; thus the continuous signal is multiplied with the Shah function; the continuous Fourier transform is again a Shah function [18]:

$$\mathsf{d}(t) = \frac{1}{\Delta t}\mathrm{III}\left(\frac{t}{\Delta t}\right) = \frac{1}{\Delta t}\sum_{k=-\infty}^{\infty}\delta\left(\frac{t}{\Delta t} - k\right) \circ\!\!-\!\!- \mathsf{D}(\nu) = \mathrm{III}(\Delta t\cdot\nu) = \frac{1}{\Delta t}\sum_{k=-\infty}^{\infty}\delta\left(\nu - \frac{k}{\Delta t}\right) \tag{2.8}$$

The whole discrete spectrum is repeated to infinity on both sides as a result of sampling.

6 Plots for demonstration

Figure 2.1 shows the different steps for the continuous function that occur to real data before its transformation to the spectral domain. Figure 2.2 shows the corresponding spectra. The sign of the real part is the same for the positive and the negative frequencies (mirrored at $\nu = 0$), whereas the imaginary part has an inverted sign (point symmetric with respect to $\nu = 0$). The continuous spectrum of an LFS sine runs through all frequencies, thus this example shows a monofrequent sine ($b_0 = 0.0\,\mathrm{Hz/s}$).

7 The spectrum of the combined expression

The four components introduced above are multiplied in the time domain. To get the spectrum of the product, the Fourier transform has to be applied to it or the Fourier transform of the components is calculated and their results are convolved afterwards [19].

$$\mathsf{srhd}(t) := \mathsf{s}(t)\cdot\mathsf{r}(t)\cdot\mathsf{h}(t)\cdot\mathsf{d}(t) \circ\!\!-\!\!- \mathsf{SRHD}(\nu) := \mathsf{S}(\nu) * \mathsf{R}(\nu) * \mathsf{H}(\nu) * \mathsf{D}(\nu) \tag{2.9}$$

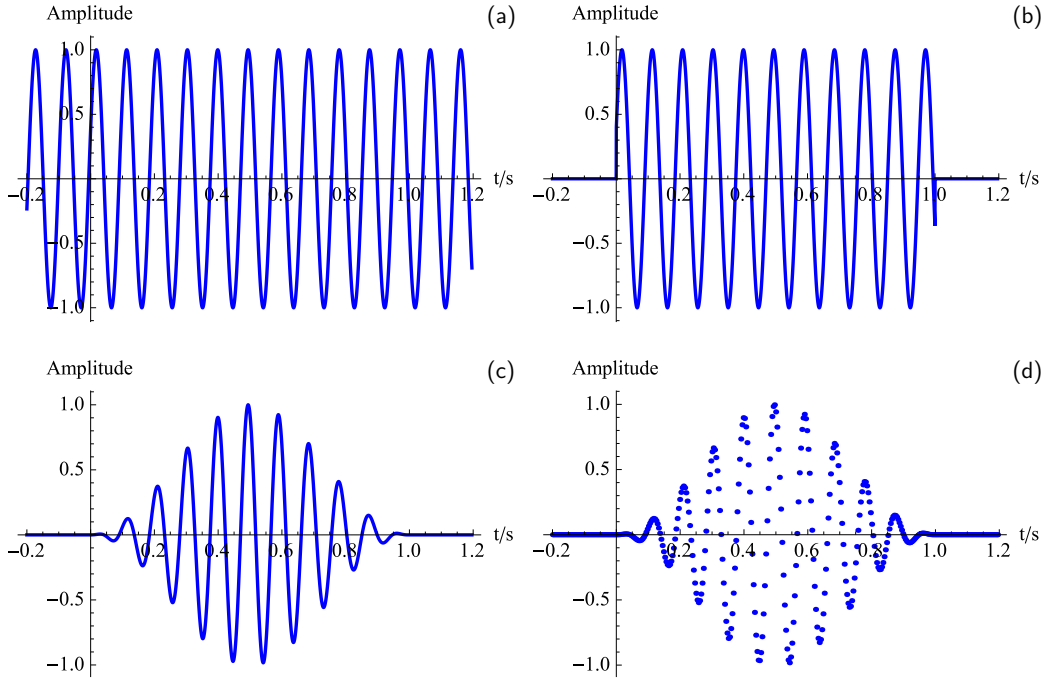

Figure 2.1.: Demonstration of the components used before transformation to the spectral domain. (a) shows the continuous function with the parameters: $A_0 = 1.0$, $\nu_0 = 10.5\,\mathrm{Hz}$, $b_0 = 0.0\,\mathrm{Hz/s}$ and $\phi_0 = \pi/8$; (b) after application of a rectangle with $T = 1.0\,\mathrm{s}$; (c) after application of the Hann window function and finally (d) after discretising (with 256 samples in the interval of the rectangle).

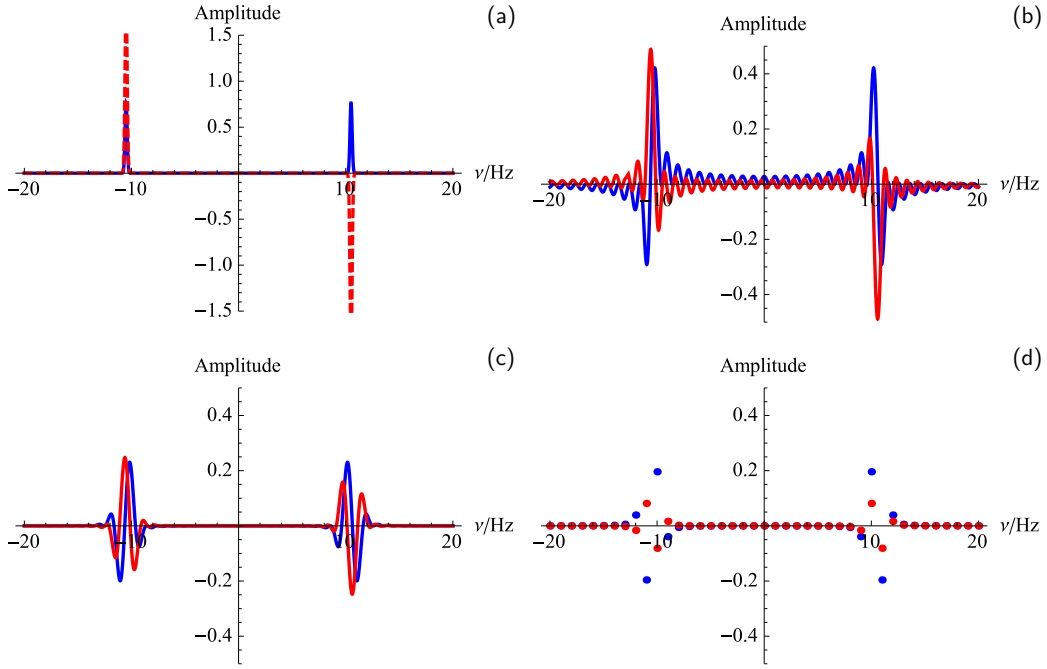

Figure 2.2.: The spectra of the plots shown in Figure 2.1 (real part blue, imaginary part red). (a) shows an approximation for the continuous-time Fourier transform of the monofrequent sine wave (the real peak would be infinitely narrow, furthermore the amplitudes of the Dirac delta functions are meaningless as they are irregular distributions and only valid if integrated); (b) after application of a rectangle; (c) after application of the Hann window function (spectral leakage decreased but peak width increased). (d) shows the discrete Fourier transform after the data are sampled (divided by N).

The derivation is tedious; two representations turned out to be particularly useful:

$$
\begin{aligned}
&\mathsf{F}(A_0,\nu_0,\phi_0,b_0,T,\Delta t,\nu) = \\
&-\frac{1}{4}\,\mathsf{SRD}_{\mathsf{pos}}\Big(\quad A_0,\quad \nu_0,\quad \phi_0,\quad b_0,\quad \Delta t,\quad T,\quad \nu-\frac{1}{T}\quad\Big) \\
&+\frac{1}{2}\,\mathsf{SRD}_{\mathsf{pos}}\Big(\quad A_0,\quad \nu_0,\quad \phi_0,\quad b_0,\quad \Delta t,\quad T,\quad \nu\quad\Big) \\
&-\frac{1}{4}\,\mathsf{SRD}_{\mathsf{pos}}\Big(\quad A_0,\quad \nu_0,\quad \phi_0,\quad b_0,\quad \Delta t,\quad T,\quad \nu+\frac{1}{T}\quad\Big) \\
&-\frac{1}{4}\,\mathsf{SRD}_{\mathsf{pos}}\Big(-A_0,-\nu_0,-\phi_0,-b_0,\quad \Delta t,\quad T,\quad \nu-\frac{1}{T}\quad\Big) \\
&+\frac{1}{2}\,\mathsf{SRD}_{\mathsf{pos}}\Big(-A_0,-\nu_0,-\phi_0,-b_0,\quad \Delta t,\quad T,\quad \nu\quad\Big) \\
&-\frac{1}{4}\,\mathsf{SRD}_{\mathsf{pos}}\Big(-A_0,-\nu_0,-\phi_0,-b_0,\quad \Delta t,\quad T,\quad \nu+\frac{1}{T}\quad\Big).
\end{aligned}
\tag{2.10}
$$

With:

$$
\mathsf{SRD}^{\mathsf{lfs}}_{\mathsf{pos}}(\nu) = -\mathrm{i}\frac{1}{4}\cdot A_0\cdot \mathrm{e}^{\mathrm{i}\phi_0}\cdot\sum_{k=0}^{N-1}\sum_{l=k}^{k+1}\mathrm{e}^{\mathrm{i}\pi l\Delta t(l\Delta t b_0-2\nu+2\nu_0)}
$$

in general, and:

$$
\mathsf{SRD}^{\mathsf{mono}}_{\mathsf{pos}}(\nu) = -\mathrm{i}\frac{A_0}{2}\sin\left(\pi T(\nu-\nu_0)\right)\cdot\cot\left(\pi\Delta t(\nu-\nu_0)\right)\mathrm{e}^{-\mathrm{i}(\pi T(\nu-\nu_0)-\phi_0)}
$$

for $b_0 = 0.0\,\mathrm{Hz/s}$ in particular. In the latter case the sums are not necessary, greatly reducing computation effort. The first derivatives are required in order to use the Levenberg-Marquardt algorithm; these are described in [14] as well as the series expansions for poles in the $\mathsf{SRD}^{\mathsf{mono}}_{\mathsf{pos}}(\nu)$.

3 Preparations for real signal analysis

I Introduction

Two theoretical examples of the derived expression (Eq. 2.10) are given in Figure 3.1. The spectral magnitude is proportional to the parameter A_0, the peak width increases with $|b_0|$, ν_0 together with b_0 determine the mean frequency of the peak. The sign of b_0 and the initial phase ϕ_0 determine the phase spectrum.

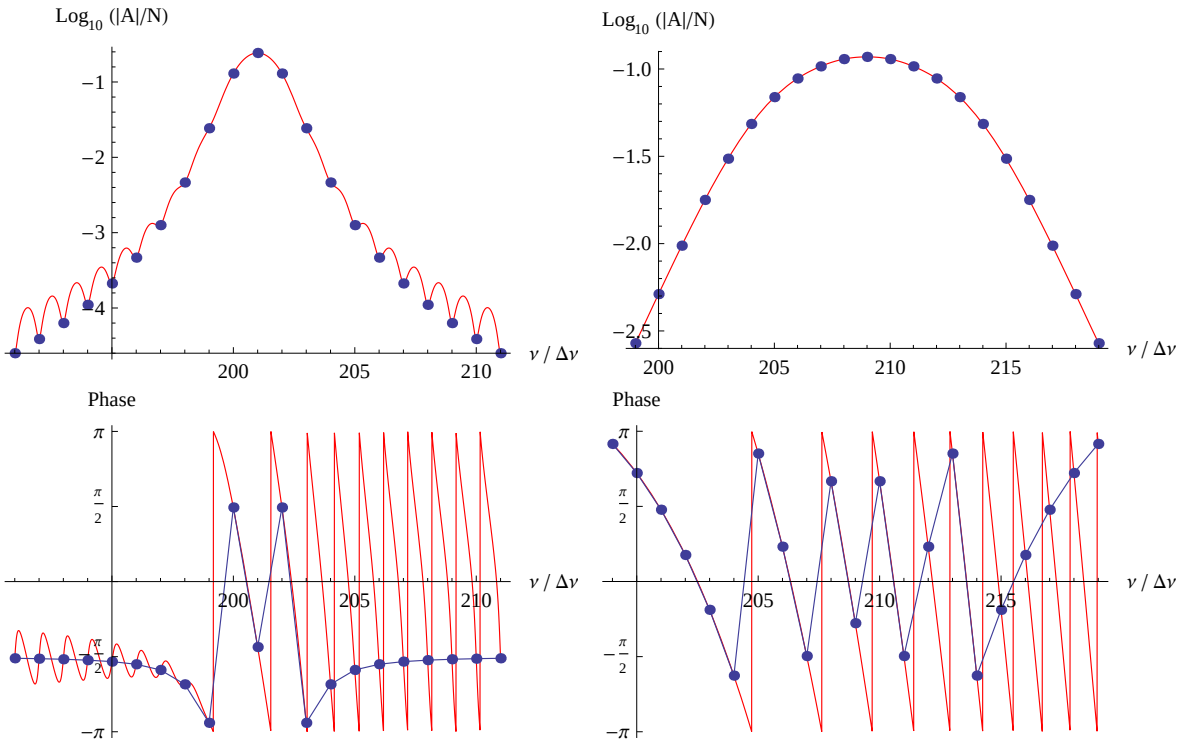

Figure 3.1.: Magnitude and phase spectra with different peak widths. Left column: $A_0 = 1.0$, $\nu_0 = 200.0\,\mathrm{Hz}$, $\phi_0 = 0.5\,\pi$, $b_0 = 2.0\,\mathrm{Hz/s}$, $\Delta\nu = 1.0\,\mathrm{Hz}$. Right column: the same but with $b_0 = 18.0\,\mathrm{Hz/s}$. Shown are the theoretical expression (Eq. 2.10) and the values of the discrete spectrum.

Spectra of real signals will contain signals from different sources and noise. The usable characteristics of periodic content will be limited to the complex values of the peaks, where the superposition with other components of the signal will be minimal. The fit algorithm requires well estimated start values for the parameters of the (LFS) sines. Another extensive part of the research is based on the identification of dependencies: how does the shape of a peak change if the input parameters change? With this understanding, the reversed dependencies allow the estimation of the parameters on the basis of the values of the peak. The dependencies and procedures are described in [14].

Figure 3.2 illustrates a typical fit for a pure LFS sine. Beyond the sixteenth digit of the fit result basically random digits follow; this limit stems from the chosen implementation of the floating-point values: in this work, double precision is used for which the numerical noise lies in this order of magnitude (≈ 16 decimal digits).

In spectra of pure artificial (Gaussian white) noise, local maxima are fitted with a wide variability of results [14]. Many test runs were done to find the receiver operating characteristic, that is the proportion of false alarms and false positives. This yielded thresholds for the (squared, weighed and summed) difference between the complex values of the peak and the fit result, χ^2_n, by allowing a certain percentage of false positives. In this work, the proportion is set to $5\,\%$, meaning that of all local maxima in a spec-

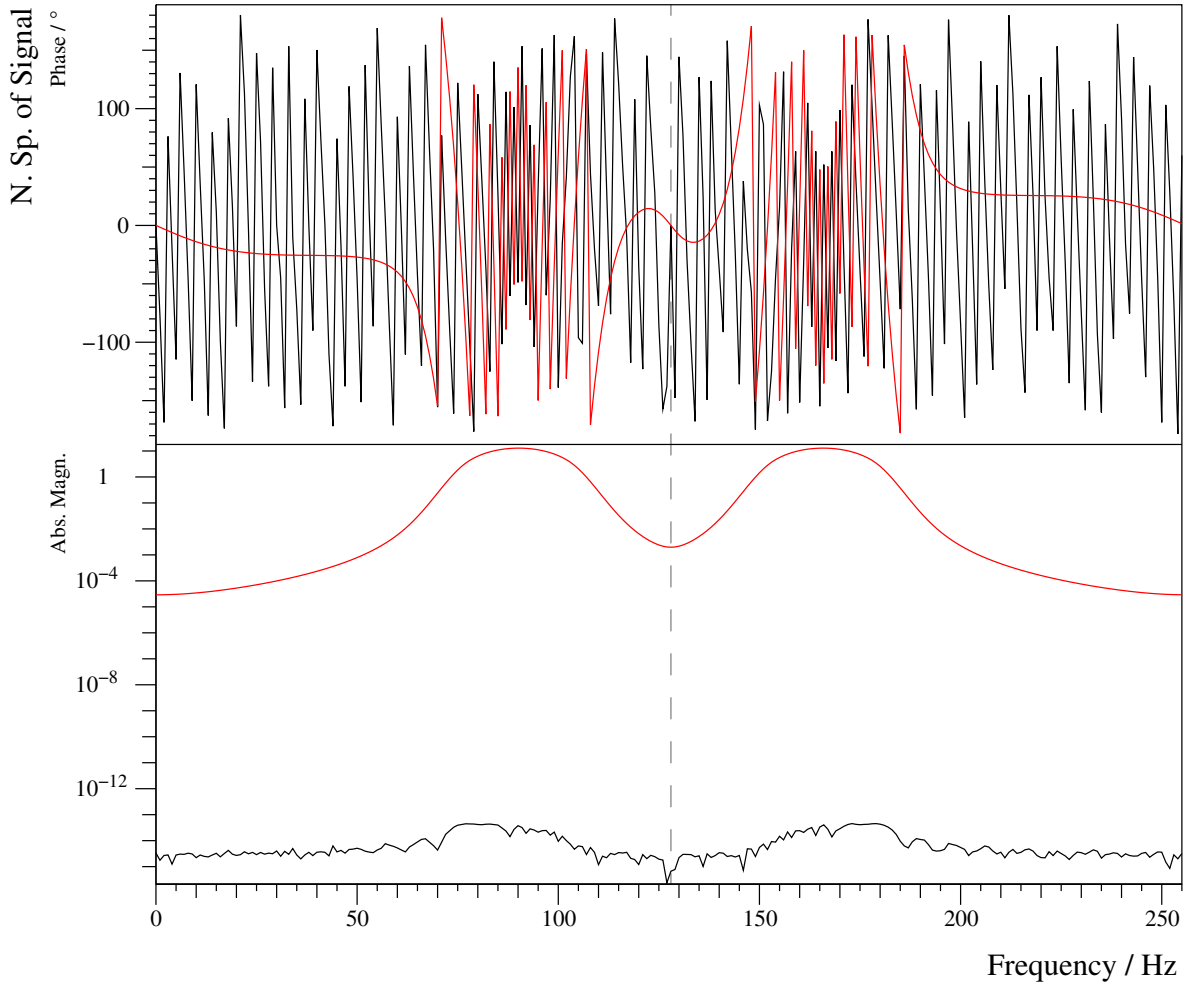

	ν_0 / Hz	b_0 / (Hz/s)	ϕ_0 / °	A_0
Input:	70.1	40.1	160.1	100.0
Start:	69.93	40.41	177.2	98.1
Fit:	70.099999999999994	40.100000000000001	160.09999999999983	100.00000000000021

Figure 3.2.: Magnitude (bottom) and phase (top) spectrum of a pure LFS sine (red) and the same after an LFS sine (Eq. 2.10) is fitted and subtracted (black), $N = 256$, $\Delta t = (1/N)\,\mathrm{s} \to \Delta\nu = 1.0\,\mathrm{Hz}$. The start-value-estimation procedure decided that 21 complex values lie within the peak width; the fitting ends after 53 iterations with $\chi^2_n = 7.92 \cdot 10^{-29}$. Beyond the Nyquist frequency ($128\,\mathrm{Hz}$) the negative frequencies are arranged. Especially the phase spectrum (top) suggests that the remaining signal mainly consists of random numbers.

trum of noise every 20^{th} peak is subtracted wrongly. The impact of small numbers of wrongly subtracted peaks on the data is small and acceptable. These χ^2_{Thres} values are a function of the number of complex values used for the fit (n_{Fit}) and decrease with increasing peak widths because the probability of the occurrences of small values of χ^2 decreases with more values being fitted.

II A real signal superposed with synthetic sines

Before analysing completely real signals with periodic disturbances, synthetic sines are superposed with a real signal. This signal is a coal-mine-induced event in the area of Hamm-Herringen, Germany [20][12] acting as a model for a substantially non-periodic aftershock signal (Fig. 3.3). It is superposed with artificial sine functions of different frequencies, frequency-change rates, amplitudes and phases as an example for periodic disturbances. The sampling rate for these data is 200 Hz and the segment length is 15 s; all examples will be performed with $1,024$ samples containing the centre part of the signal.

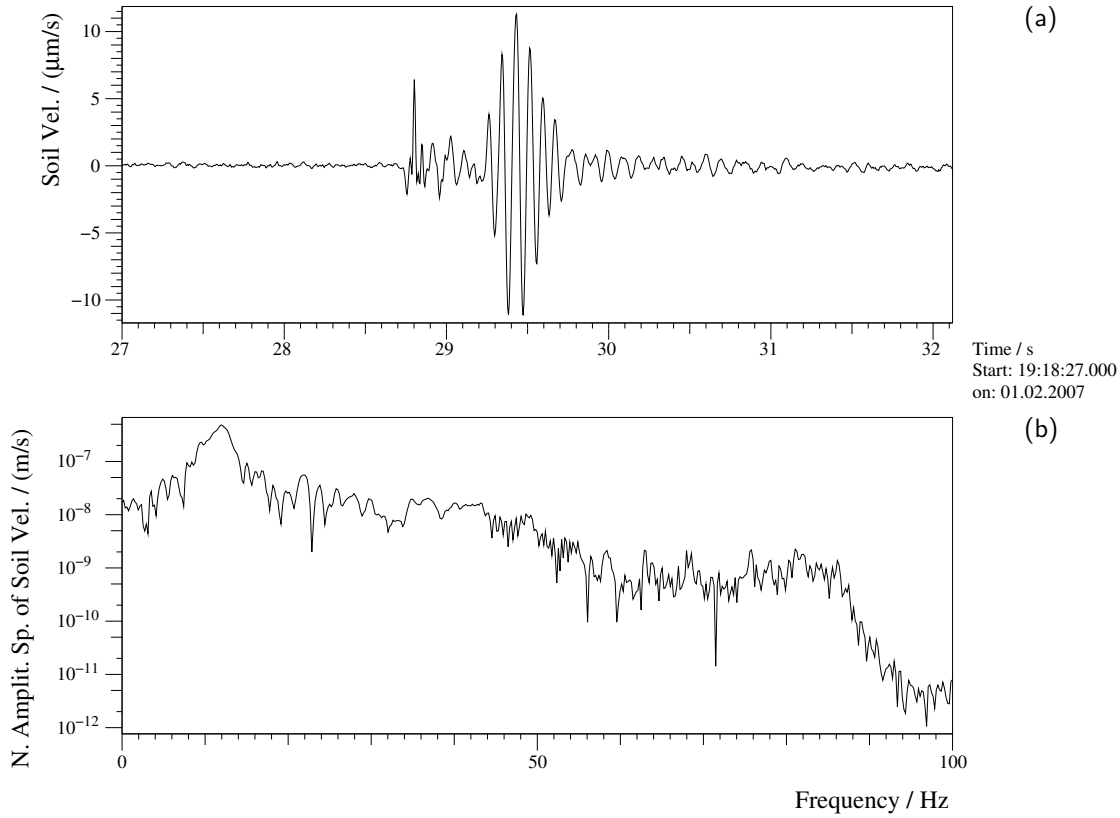

Figure 3.3.: Test signal from a coal-mine-induced event. (a) shows the time-domain signal ($1,024$ samples at $200\,\text{Hz}$) which will be superposed with artificial sines to test the algorithm. (b) is the magnitude spectrum of the same signal.

12 Data kindly provided by Monika Bischoff and Sebastian Wehling-Benatelli (Institut für Geologie, Mineralogie und Geophysik; Ruhr-Universität Bochum). Measured: 1. February 2007, 19:18:28 UTC during the "HAMNET" acquisition period. Location depth is 1,056 m, distance between source and sensor 1,441 m, Mercalli intensity: -0.48, vertical component of a 3D-velocity sensor.

1 First example

The signal of Figure 3.3 is superposed with a single LFS sine;[13] the input parameters and fit results are shown in Figure 3.4. $N = 1{,}024$ samples are used for the FFT, then an LFS sine is fitted to the highest maximum. In this example, the algorithm stops after 39 iterations with: $\chi_n^2 = 7.646 \cdot 10^{-4}$, which is not as low as in the synthetic case because the peak form is slightly modified by the event signal. The number of complex values used for this fit is $n_{\mathsf{Fit}} = 28$.

By applying the inverse FFT, the signal is restored with very few changes (b); the strongest changes occur at the beginning of the time interval in the order of 5 % peak-to-peak, referred to the maximum of the event.

2 Bigger amplitudes

The sine of the example above is increased in amplitude, while the procedure remains the same. Two examples for the factors 100 and 10^4 are demonstrated in Figure 3.5. In the spectra one can see fluctuations in the regions where the spectra of the LFS sine and the underlying signal are in the same order of magnitude. Although both curves have a smooth magnitude spectrum, their phases fluctuate strongly, causing ripples if added. In all other regions the spectrum of the signal dominates, so the sum spectrum shows the respective smoothness.

The superposition is achieved by adding two complex values: As long as the sine is considerably stronger than the other signal, a further amplitude increase does not change the phase significantly. Therefore, no significant changes of the shape of the difference signal can be expected, as long as the fitting and subtraction quality is sufficient to lower the sine peak below the level of the superposed signal. Figure 3.6 compares three examples of different amplitudes: The χ_n^2 becomes better – pretty much in the same way that the amplitude increases: χ_n^2 contains the squared differences; for every amplitude increase by a factor 100, χ_n^2 decreases approximately by a factor of 10^4. On the one hand the fit quality increases, on the other hand relatively more has to be subtracted to reach the same level of remaining signal.

To conclude: There is no such thing as a proportionality of the amplitude of the sine and the error that remains in the data. As long as the peak of the sine is clearly higher than the underlying signal, the deviation is more or less the same. Instead, the biggest contribution to the RMS_Δ stems from a notch which is likely to remain in the spectrum after subtraction of the sine.[14] Its "size" depends mainly on the phase spectrum of the underlying signal in combination with the sine parameters – with very little influence of the amplitude (as shown in Fig. 3.6).

3 Bigger linear frequency shift

This example demonstrates the performance of the algorithm, if the added sine has a very strong linear frequency shift. The parameters and results are given in Figure 3.7.[15] As described, the sampling rate is 200 Hz, $1{,}024$ samples are used in the FFT, therefore the frequency increases from 10.00 Hz to $10.00\,\mathrm{Hz} + 16.00\,\mathrm{Hz/s} \cdot 5.12\,\mathrm{s} = 91.92\,\mathrm{Hz}$ in the chosen time interval. (a) and (b) demonstrate that the deviations from the original signal are low and in the same order as with the narrower peaks in the last section ($RMS_\Delta = 1.48781 \cdot 10^{-7}$). By this procedure, smaller magnitude values are altered relatively more than big ones; this is reasonable as for the χ^2 parameter in the fit procedure, the sum of the squared differences – in which all differences are weighted the same – is minimised.

13 An example of a real signal containing a seismic event and mains hum is briefly described and published on a poster [21].

14 By fitting sine parameters to superposed spectra, the algorithm tends to subtract more power (not mandatorily equal to a bigger A0) than the power of the pure sine contained. As a consequence, notches show up in the remaining spectrum.

15 Further fit properties are: $\chi_n^2 = 1.6530 \cdot 10^{-9}$ after 38 iterations; 211 complex values are used, centred at index 261.

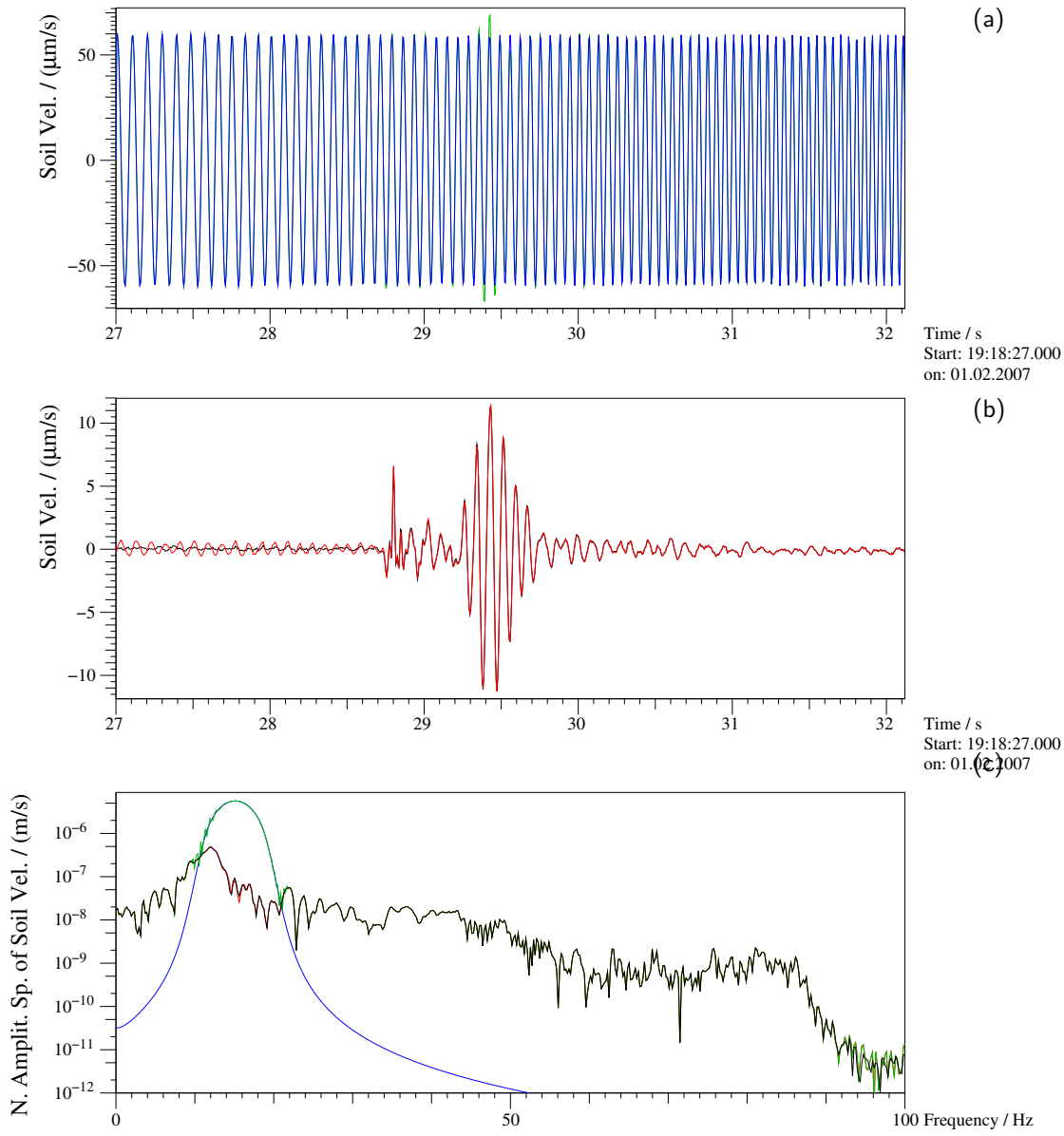

	A_0	ν_0	b_0	ϕ_0
Input	$50.0\,\mu\mathrm{m/s}$	10.0 Hz	2.0 Hz/s	$1.0\,\mathrm{rad}$
Fit result	$49.9964\,\mu\mathrm{m/s}$	9.999311 Hz	2.000154 Hz/s	$1.01019\,\mathrm{rad}$

black	Original signal
green	Signal superposed with sine
red	After subtraction of the sine
blue	Sine with the parameters of the fit result

Figure 3.4.: Test signal from a coal-mine-induced event superposed with an artificial LFS sine. (a) and (b) illustrate the time domain; both plots contain two signals according to their scale. (c) shows all four spectra in a logarithmic plot. Note that the coloured curves often cover each other.

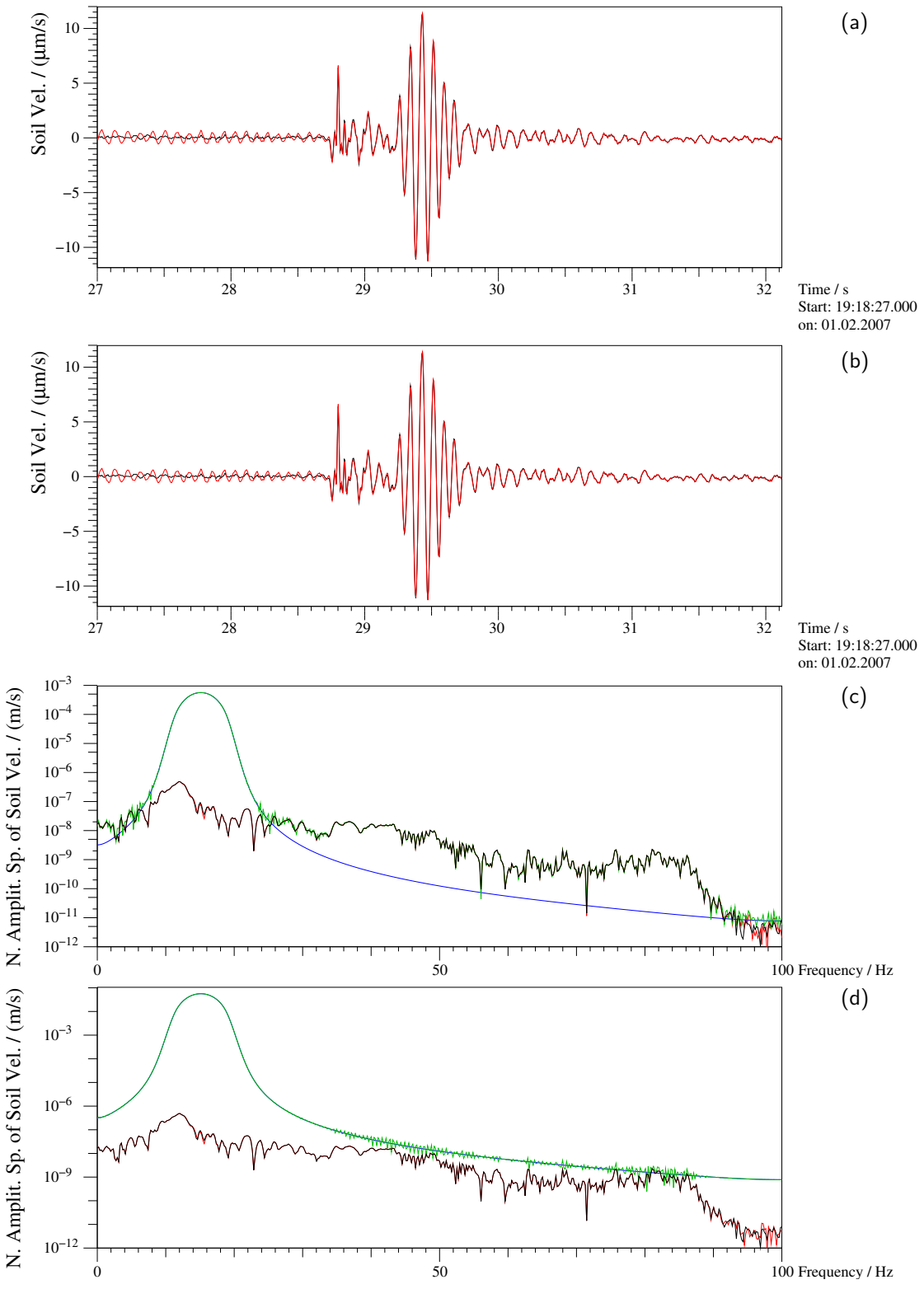

Figure 3.5.: Test signal from a coal-mine-induced event superposed with an artificial LFS sine. (a) and (b) illustrate the same original and restored signal as Figure 3.4 (b) but with the sine amplitude increased by a factor of 100 resp. 10^4. (c) and (d) show the corresponding spectra (similar to Fig. 3.4 (c)).

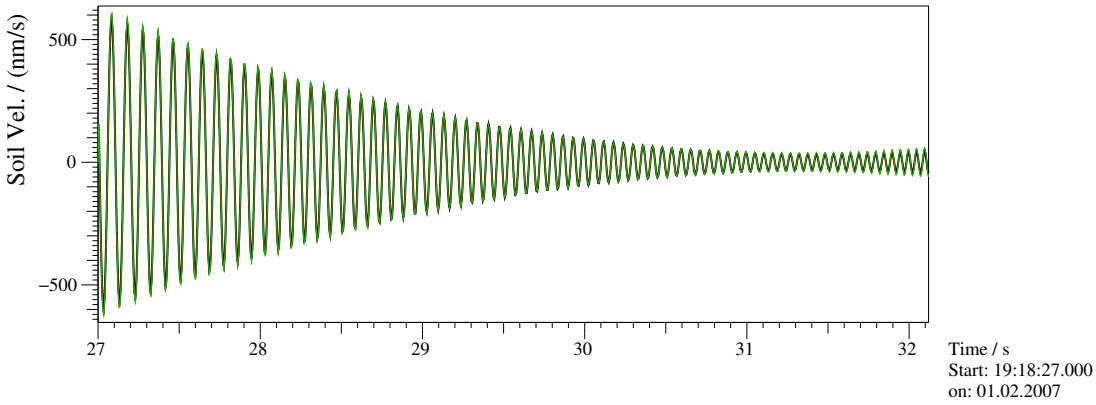

Amplitude factor	#Iterations	#Compl. values	χ^2_n	RMS_Δ
1	39	28	$7.6462 \cdot 10^{-4}$	$1.85684 \cdot 10^{-7}$
100	39	28	$7.5283 \cdot 10^{-8}$	$1.91219 \cdot 10^{-7}$
10^4	32	28	$7.5271 \cdot 10^{-12}$	$1.91246 \cdot 10^{-7}$

Figure 3.6.: The deviations between the reconstructed and the original signal: the curves are pretty much the same. In order to quantify the influence of the LFS-sine subtraction on the data the RMS_Δ value is used as a measure for the power difference between the original signal and the signal after subtraction of an (LFS) sine. For artificial signals, the signal without (LFS) sine is known and can be compared with the signal after an (LFS) sine is added, fitted and subtracted. These two signals are subtracted from each other and the root mean square (RMS) value is determined in the time domain; ideally it would be zero.

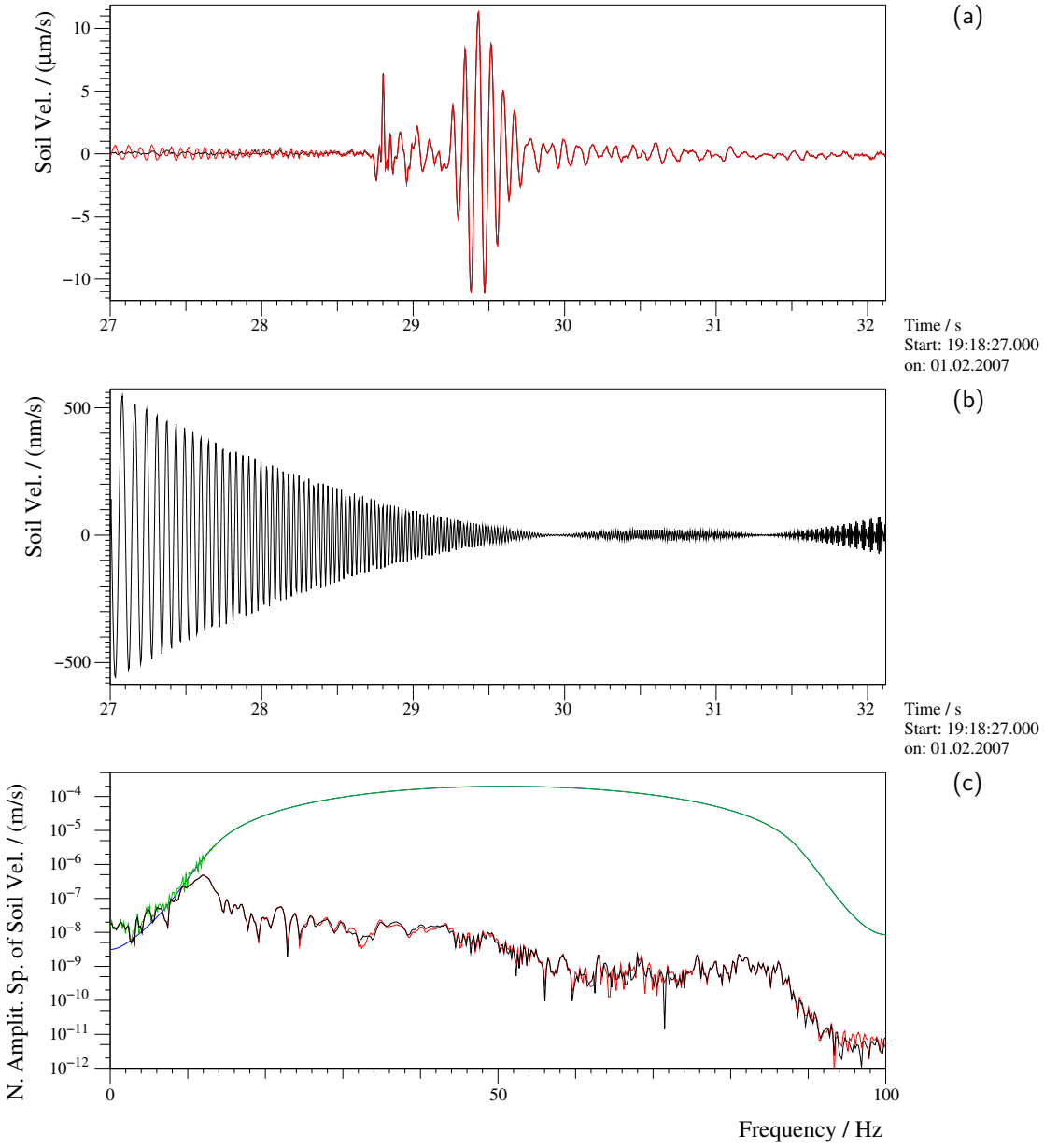

	A_0	ν_0	b_0	ϕ_0
Input	$5.0\,\mathrm{mm/s}$	$10.0\,\mathrm{Hz}$	$16.0\,\mathrm{Hz/s}$	$1.0\,\mathrm{rad}$
Fit result	$4.9999981\,\mathrm{mm/s}$	$9.9999912\,\mathrm{Hz}$	$16.000002413\,\mathrm{Hz/s}$	$1.000096\,\mathrm{rad}$

black	Original signal
green	Signal superposed with sine
red	After subtraction of the sine
blue	Sine with the parameters of the fit result

Figure 3.7.: Test signal with superposed LFS sine of high frequency-change rate. (a) shows the time-domain signal of the original signal and after sine addition, fitting and subtraction. (b) shows the difference between the two signals. (c) shows all four spectra, just like in the former example.

4 Analysis of real data

I Introduction

In this chapter, sine subtractions from longer time intervals of data are demonstrated. For this purpose, sequences of complex spectra are generated from the data that shall be cleaned from periodic disturbances. Yet, no spectra-overarching analysis is provided, and the single spectra are processed separately.[16] For each time interval, the spectrum is calculated and the locations of the local maxima (the peaks) of the magnitude are extracted. These are sorted by amplitude (in decreasing order) and again processed one by one: the start values are estimated and if the subsequent fit is successful, an (LFS) sine with the fit parameters is subtracted from the single, complex spectrum. When all peaks in all spectra have been processed, the sequence can be transformed back into the time domain. Much effort was spent to make the processing run automatically and provide clear presentations of the outcomes.

1 Additional features of the final algorithm for removal of (LFS) sines

Some refinements are necessary in order to avoid rarely occurring cases in which the fit algorithm gets stuck in secondary minima, uses too much computation time, returns not physically plausible results or the like. The most important enhancements are described in the following:

a A special approach for small peak widths

Admittedly, the $\mathsf{F}_{\mathsf{Sum}}$ expression can handle monofrequent sines but it has one parameter (b_0) more than the $\mathsf{F}_{\mathsf{Mono}}$ expression. The probability, that the underlying signal / the noise fits well to the spectrum of a certain LFS sine by chance if very few spectral values are used, is considerably higher if one more fit parameter is available. This fact leads to an increased rate of false positives for the $\mathsf{F}_{\mathsf{Sum}}$ expression compared to $\mathsf{F}_{\mathsf{Mono}}$. Lowering the $\chi^2_{\mathsf{Thres}}(n_{\mathsf{Fit}})$, however, leads to an increased false-negative rate; the better approach is to use $\mathsf{F}_{\mathsf{Mono}}$ in the case of narrow peaks. On the other hand, small values of $|b_{0,r}|$ can also produce narrow peaks. Therefore a categorical approach, namely the usage of $\mathsf{F}_{\mathsf{Mono}}$ for each narrow peak, is not reasonable. Instead, in the case where the start-parameter estimation suggests to use three complex values for the fit, the following sequence is carried out:

- The $\mathsf{F}_{\mathsf{Mono}}$ fit is done.
- The $\mathsf{F}_{\mathsf{Sum}}$ fit with three parameters is done with its strict $\chi^2_{\mathsf{Thres}}(n_{\mathsf{Fit}} = 3)$.
- The $\mathsf{F}_{\mathsf{Sum}}$ fit with one added value to the right is done with the weaker threshold for $n_{\mathsf{Fit}} = 4$.
- This is done with an additional value to the left analogously.

For any fit fulfilling its specific threshold criterion, the resulting χ^2_n value is divided by its individual threshold. The lowest ratio indicates the best result and an LFS or monofrequent sine with the corresponding parameters is subtracted.

Depending on the position of the ν_0 on the raster of discrete frequencies, a monofrequent sine can have three or four strong magnitude values. Therefore, if four complex values are chosen by the start parameter estimator both – the monofrequent as well as the $\mathsf{F}_{\mathsf{Sum}}$– expressions are fitted to these four points. Again, the one with the better ratio ($\chi^2_n/\chi^2_{\mathsf{Thres}}(n_{\mathsf{Fit}})$) is chosen.

16 An optimised algorithm should use fit results of at least one spectrum and expect a similar sine in the neighbouring time intervals. Checking for consistency can also help to discard false positives that occur in just one spectrum.

b Avoidance of fit results for much broader peaks than expected

In rare cases, the fit was performed successfully starting with few complex values – which suggests a narrow peak – but ends up with a very high value for $|b_0|$. With increasing $|b_0|$ the magnitude of the peak drops, thus sets of parameters with high values for A_0 and $|b_0|$ can be observed. The subtraction of the corresponding broad and strong peaks from the spectrum, in which only few data points fit, causes the surrounding values to increase in magnitude much above the original ones, yielding a marked increase of power in the spectrum. Such a case should be avoided by all means. If this fit result was correct, its peak should fit on its whole width. Therefore, if the fitted b_0 does not fit to the estimated peak width, the fit is rerun with a higher number of complex values.

c Uncovering of hidden peaks

If a peak is subtracted, its complete spectrum is subtracted. Significant changes occur for the values of the peak and the surrounding. Within these values new peaks might occur or peaks, which could not be fitted successfully before, might now be subtractable. The safest way is to restart the complete procedure for the remaining spectrum after the subtraction of the single peak has been performed. This approach is very time consuming.[17] Due to the monotonous decrease of magnitude of an LFS-sine peak, its subtraction manipulates the values of the spectrum the less, the more distantly they lie from the centre of the peak. Assuming that this manipulation becomes insignificant at a certain (relative) magnitude, it is more sensible to analyse only a small spectral interval again. The strength of the decrease of magnitude with the frequency can be derived and is basically a function of $|b_0|$. With its help the interval of spectral values in which the peak analysis should be repeated is roughly estimated.

d Reconstruction of the time-domain signal

As mentioned in Section I, longer time intervals are analysed in this chapter, for this purpose sequences of spectra are processed. A longer time interval is apportioned into multiple short ones, according to the chosen number of samples per FFT (N). The application of the Hann-window function sets the first sample of each time interval zero before a FFT is performed; thus, after inverse FFT and even after the application of the inverted window function, this first value would remain zero.[18] If multiple intervals would be recombined, the result would show periodically missing samples. Furthermore, the window function decreases the weights for the outer-most values, giving the most weight to the middle. A particular reason for using considerable overlap is the trend of the errors (stemming from the notches after sine subtraction) to increase to the margins of the time interval (e.g. figures in Sec. II). By merging spectra and suppressing their outermost values, this effect can be reduced strongly. In this chapter each single spectrum overlaps by 25 % with its precursor. Thus, in the sequence plots, the time shift between two beginnings of subsequent spectra is given by:

$$\Delta T_{\mathsf{Spect}} = 0.75 \cdot N \cdot \Delta t. \tag{4.1}$$

If transformed back to the time domain, the overlapping parts are weighted in such a way that the amplitudes from the last spectrum decrease linearly and the amplitudes from the current spectrum increase

17 In this chapter the $\chi^2_{\mathsf{Thres}}(n_{\mathsf{Fit}})$ are set to allow 5 % false positives. If a spectrum consists of $4,096$ magnitude values (at positive frequencies) and approximately every fourth is a peak, then there are around 50 subtractions in each spectrum if it consists only of noise. For signals containing different fundamental frequencies with several harmonics, this number can drastically increase. Assuming that 50 peaks, which will be successfully fitted, are equally distributed in a list of $1,000$ peaks in total, then a restart is performed after every fit of one of the 50 successful fits, meaning there will be one late restart for every early restart. Thus, the average number of fits between two restarts will approximately lie at half of the complete number, namely 500. Consequently, for 50 restarts, the computational effort will be 25 times higher compared to the procedure without restarts.

18 This is an issue only concerning the first value. The annulment of the window function for other values is unproblematic: For these numbers of samples per FFT, the calculation precision at every point is significantly higher than the range of weights resulting from the Hann-window function. Even at $8,192$ samples the precision is several orders of magnitude higher than the quotient between the highest (1.0) and the lowest ($1.47 \cdot 10^{-7}$) non-zero value of the weight function – except for the first sample which will always be zero.

in the same way over the time of overlap. Thus the preceding spectrum is faded out in the same way as the next spectrum is faded in, keeping the proportions right.

2 Seismic and acoustic data

Even though the work is motivated by subtracting periodic noise from seismic signals, most of the following examples use acoustic data. It is much easier to find or generate periodic acoustic than seismic signals.[19] If acoustic signals couple to the ground, a significant amount of energy is reflected or absorbed causing the SNR to be considerably higher in acoustic data. Typically, compared to acoustic signals, seismic signals are complexer in the time domain (mainly because of reflections at soil-layer boundaries,[20] additional seismic wave types[21] or, for surface waves in a layered medium, even a significant influence of dispersion); mainly, they show multiple arrivals of an event, caused by the multiple propagation paths and different propagation speeds of the wave types. However, the corresponding spectra remain relatively simple; the mentioned effects influence the spectral amplitudes and phases, but the frequencies stay the same.[22]

The interference between the directly measured signal and signals propagating along indirect paths can be destructive or constructive, depending on the differences of their path and wave lengths. The self-interfered signal will show time dependent variations in its magnitude if either the relative path length or the frequency changes significantly within T; both cases are not covered by the algorithm.

The present approach works with all kinds of data, including the acoustic or seismic ones, recorded in our group. Because of the better SNR most of the evaluated signals shown in the following sections stem from acoustic measurements.

3 Number of samples per spectrum

The number of values forming a peak in the frequency domain increases quadratically with the number of samples of the Fourier transform: For a bigger number, the elapsed time T is longer, meaning that the end frequency has evolved farther away from the start frequency. In addition, the resolution in the frequency domain increases linearly with N, so more values are available in a given frequency interval.

As long as there are no significant changes of the frequency higher than to the first order, there are two arguments for a high number of samples: Firstly, the algorithm for broad peaks is to be tested with priority, therefore challenging conditions (with high values of b_0) are preferable. Secondly, the peaks have to be well separated; for this a suitable spectral resolution is required.

The precondition that the signal is sufficiently homogeneous usually is appropriately fulfilled if the time interval per spectrum is less than 1 s. The number of values in this work is $8,192$ samples for sampling rates of 10 kHz or $4,096$ if the sampling rate is slightly smaller.

4 False-positive rate

In the following evaluations 5 % false-positive fits are accepted (this means: in a spectrum of Gaussian white noise 5 % of all peaks are classified as originated by sines and subtracted). As a consequence,

19 One can use a sound card with a speaker and play a simple audio file. Beside possible non-linearities in the transfer function of the hardware, a weak disadvantage of acoustic signals is the fluid propagation medium: the speed of sound (measured on the ground) can be time dependent (e.g. wind). Acoustic waves excite seismic waves if hitting surfaces – but with reduced amplitudes. The direct excitation of strong periodic seismic waves is more complicated; typically, special devices are operated, like vibrator trucks or smaller plate vibrators.

20 The seismic-wave propagation depends on many factors, among others the kind, porosity and layering of the soil, the groundwater level etc. [22, Chap. 9]. Changes in the wave speeds between different layers reflect and refract the wave.

21 Compressional and shear waves, surface waves (Rayleigh, Love waves) [22, Chap. 2].

22 Signals may become complicated if an interfering LFS sine gets independently changing frequencies, e.g. if one propagation path hits a moving reflector, that part of the signal becomes Doppler-shifted and the superposed spectrum consists of doubled peaks, which can cause the algorithm to fail.

many peaks will be subtracted; reasonable limits and conditions could be thought of for sorting out candidates for sines and to strongly reduce this percentage. Their implementation would result in more parameters that had to be described and motivated which would go beyond the scope of this work. Ideas are listed in Chapter 5. To demonstrate the performance of the fit algorithm this rate of 5 % false positives is accepted. Furthermore, the cursory analysis of the influence of sporadically subtracted erroneous (LFS) sines from data shows that the resulting modifications seem to be insignificant to non-periodic events in the data.[23]

II Main battle tank

We fortunately have access to seismic and acoustic data of passing military vehicles. These data had been measured between 1989 and 2001 by the Bochum Verification Project (BVP) [23] which is continued as the Group Physics and Disarmament at TU Dortmund in which this work has been done. Ground vehicle noise and vibration are a second source of disturbing signals expectable during OSI. In particular on military ground tracked vehicles may be used. Compared to wheeled vehicles, tracked ones have an additional strong source of periodic noise: Beside the engine in general, the interlocking of the driven cogwheels into the track produces a second fundamental frequency and harmonics. And the rolling of the wheels over the track elements with corresponding variable forces to the ground produces seismic vibration at these frequencies directly.[24]

In Amersfoort, Netherlands, (1992) the BVP together with several partner scientists from NATO and WTO countries measured the seismic and acoustic emissions of military vehicles. Here, an example of a `Leopard-1` main battle tank (MBT) driving with 11.2 $^{\mathrm{m}}/_{\mathrm{s}}$ on a straight road (paved with smooth asphalt) is analysed at a distance of 11.78 m from the designated middle of the lane.[25] The acoustic spectra consist mainly of two fundamental frequencies and their respective harmonics, stemming from the exhaust and the track drive. $4,096$ samples corresponding to $0.5622\mathrm{s}$ are used for each spectrum as a compromise between spectral and time resolution.

Figure 4.1 (a) shows three sequences of magnitude spectra from the complete time interval that is analysed (time on the mantissa). The frequency is plotted on the ordinate; the magnitudes of the spectral values of the sound pressure are given in the grey scale: With seven orders of magnitude almost the full range is presented.[26] One can see that the amplitudes are highest around 11:58:19. At this time the tank had passed the sensor. This matches the visible change of the Doppler shift: The horizontal lines progress like a negated arctangent, caused by the source during its linear trajectory moving towards, passing and moving away from the sensor. Since the tank signals are strongest at low frequencies and for the sake of clarity (a) shows the lower 500 Hz of the sequences of the spectra: before (bottom) and after subtraction (middle) of sines. The theoretical spectrum (top row) is the sum of the subtracted sines and thus, the sum of the two top spectra is equal to the bottom one.

Figure 4.1 (b) gives details on the fits. Like (a) it is the sequence of the subtracted spectra but a different illustration: each subtracted sine is represented by a circle (under the condition that its amplitude is at least 10^{-4} times the strongest of all amplitudes) at the mean frequency of the peak ($\nu_0 + 0.5 \cdot b_0/\Delta\nu$).[27] The colour codes stand for the different paths the fit procedure can take: Black circles indicate that the estimated peak width includes at least four complex values and the fit with the $\mathrm{F}_{\mathrm{Sum}}$

23 We are not trained in analysing seismic wave forms. Details might get lost, but by visual inspection the worst case that happened is: a decrease in the order of a few per cent of the peak-to-peak value in the time domain at the time of an event accompanied by small additional oscillations increasing to the margins of the time interval, see e.g. Fig. 3.4 (b) in Sec. II. The small decrease of the peak amplitude in the time domain can hardly be seen. If multiple subtractions are performed within the frequency range of the (broadband) underlying signal the effect increases.

24 Wheeled vehicles can also produce a second series of peaks caused by a coarse tyre profile, but with much lower amplitude [23], [24].

25 The experiment is described and evaluated with regard to vehicle classification in [23] and [15]. File: `AME10215.DA6`, Microphone `BK3`, `Brüel & Kjæer 4188`, with preamplifier 2639, height above ground: $20\,\mathrm{cm}$, channel $\#13$ ADC `Microstar DAP 2400/5`, sampling frequency 7,286 Hz, cut-off frequency 300 Hz.

26 Within these seven orders of magnitude all significant values are presented. Showing the full scale is not useful: By chance arbitrarily small values can occur, reducing the resolution on the logarithmic grey scale likewise arbitrarily.

27 Again, this limitation of visualised results is reasonable to focus on the strongest peaks with the highest impact on the signal.

expression was successful. If the fit results in a $|b_0|$ much broader than expected, it is rerun with more complex values (Sec. b), this case is shown in purple. The other colours (explained in the figure margin) mark the different outcomes for narrow peaks (Sec. a); in most cases the monofrequent approach (F_{Mono}) produces the best result.[28] The amplitude is given in the diameter (also here with logarithmic scaling), so bigger circles have a higher relevance.

Figure 4.1 (c) demonstrates the RMS values as a measure of the power in the data. One time is marked by a vertical line: Here the factor for the reduction of power by sine subtraction is minimal. The sequence of theoretical spectra ((a), top) is especially suitable for understanding the curve progression of the RMS values. When the former has many bright dots, much power is subtracted. The spectrum marked (at 11:58:17.8) contains some of the strongest peaks even after the subtraction of sines, the spectrum and the corresponding time-domain interval are given in Figure 4.2; this one is given in detail because it shows both: peaks that are successfully subtracted and others that remain in the spectrum.

Strong non-periodic contributions remain in the signal, however, so that the RMS amplitude of the signal was reduced by a factor of approximately 3. Most of the strong peaks in the spectra are subtracted successfully but also many remain. Superpositions of harmonics of the two series occur which are likely to form peaks that cannot be separated and fitted with the expression for a single sine. Especially, the spectrum shown in Figure 4.2 contains peaks with no obvious distortion while having a strong magnitude. During this time, the tank is close to the sensor and the superposition conditions of different sources change most strongly. One can speculate whether this could be caused by the superposition of sources with the same frequency – this tank has two tracks and two exhausts. Changing the position of the tank changes the differences of lengths of the propagation paths between the sources and the sensor.

28 Because of the low χ^2_n threshold for F_{Sum} as a result of one fit parameter more compared to F_{Mono} (Sec. a), green circles are very rare in general.

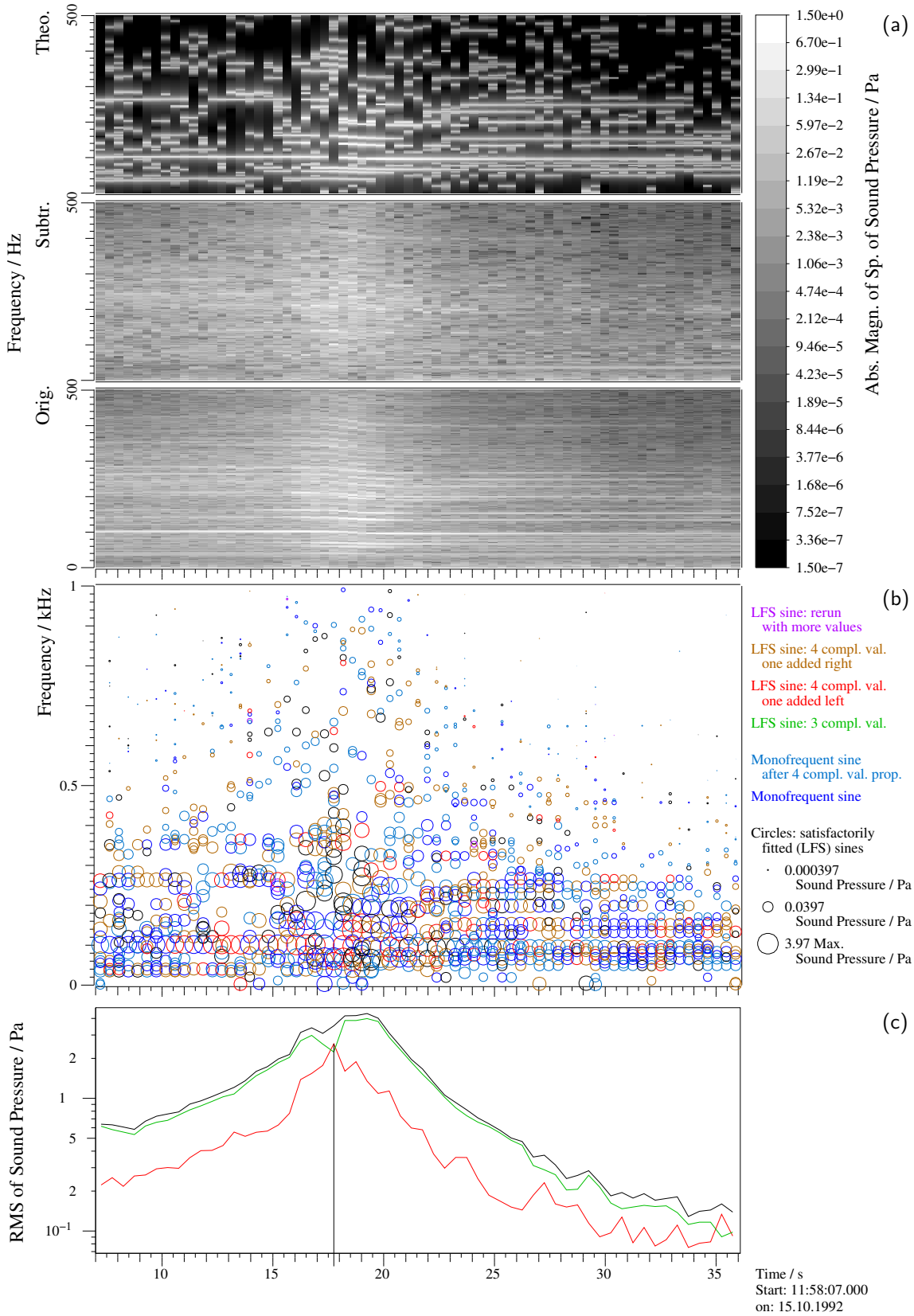

Figure 4.1.: Evaluation of a tank passing a sensor. (a) includes the three sequences of spectra: sum of subtracted sines (top), processed (middle) and original (bottom). (b) gives fit details on the subtracted peaks; (c) the corresponding RMS values (black: original data, red: sum of subtracted sines, green: processed data).

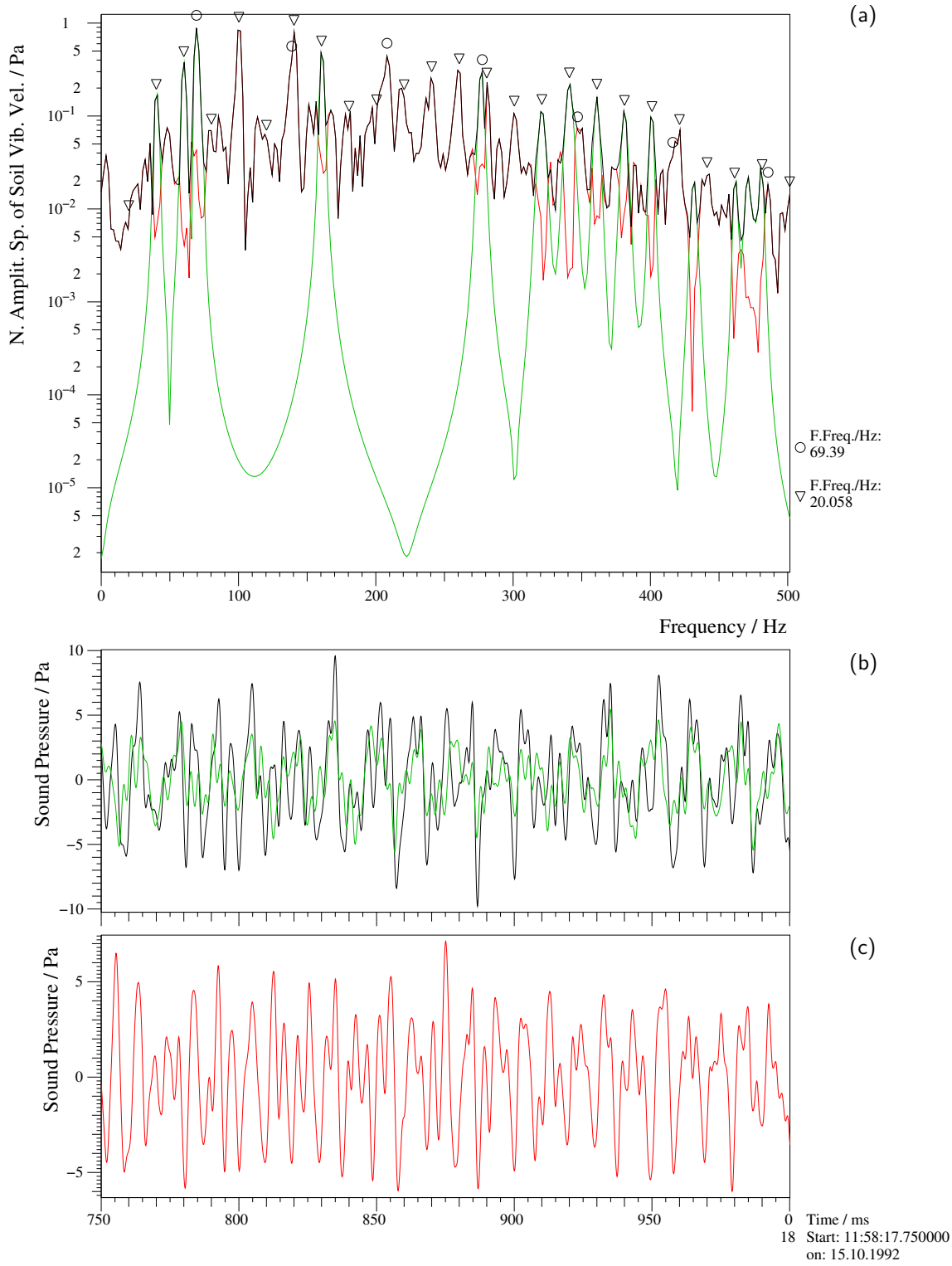

Figure 4.2.: Example for a spectrum and the reconstructed time interval with the lowest reduction of energy (see Fig. 4.1 (c), at 17.75 s). (a): spectrum, (b): time domain of the original signal (black) and the sum of subtracted ones (green). (c): the remaining signal (red).

III Additional sources of signals

Similar to the data of the MBT, acoustic and seismic signals from different sources have been processed, i. e. propeller aircraft, helicopters, a sawmill, mains hum and synthetic sounds. Some more examples are published in [14].[29] The experiences made when analysing real data are summarised in the following:

In the case of narrow peaks, the processing has been very successfully both for acoustic and seismic measurements, with the seismic data being strongly superposed with mains hum increasing the probability for a failed fit. The processed spectrum is reduced down to the background-noise level, so that only a lower threshold for the reduction factor can be derived: it is at least three orders of magnitude. For narrow and monofrequent peaks – where the transfer function is constant – the factor might be principally unlimited, as indicated for synthetic superpositions in Section II.

The broadest peaks analysed correspond to a synthetic LFS sine with $b_0 = -100.0\,\mathrm{Hz/s}$, here the peak magnitudes are reduced by 1.5 orders of magnitude only.[30] Nonetheless, the RMS value of the time-domian signal is reduced by one order of magnitude down to the level of the background at times when no sounds were played.

For the signals of vehicles, the peaks have been too narrow to observe the deviations mentioned for broad peaks. All peaks that have been fitted successfully are reduced to the level of the background, but typically several smaller and sometimes even stronger peaks remain.

Real sources, which do not produce exclusively periodic noise, are not conducive to quantifying the fit performance, for instance by the ratio of RMS before and after processing. The optimal result is a complete removal of periodic components and simultaneously no manipulation of the non-periodic content. Since the ratio of the two is unknown, there is no quantitative measure for the degree of achieving the goal. However, one can use the RMS value to find out to what extent a signal is changed during processing.

If the data are dominated by (even single) strong peaks which remain in the data, the factor of RMS-value reduction will be small – independent of the number of successfully subtracted peaks. This phenomenon was strongly pronounced for the acoustic data of the propeller aircraft – here, the signals contain very low frequencies for which the start-value estimation fails. The reduction factor of the RMS amplitude ranges from insignificant to more than 5.

If a peak shape does not match the one of a single (LFS) sine, the probability of a successful fit is small (even though sometimes by chance the χ^2_n-threshold requirement may be met) and thus, the chance of the peak remaining in the data is high. This was recognised for helicopter signals with a small distance between source and sensor. One can speculate about the reasons; by visual inspection of spectra it seems that at least two harmonic series with very similar fundamental frequencies dominate the spectrum.

29 In the cited work, additionally evaluations are introduced and performed, e.g. tracking of sines over several spectra.

30 In our recordings of synthetic sounds, we suspect the presence of a slight frequency dependency of the transfer function between the sound file on the computer and the measured data that becomes the more relevant the stronger the frequency shift in time is and deteriorates the fit quality.

5 Summary and conclusion

The Comprehensive Nuclear-Test-Ban Treaty Organization (CTBTO) can conduct an on-site inspection (OSI) if a suspicion of a nuclear explosion has arisen. Local seismic sensors detect not only potential aftershock signals of an underground explosion but also disturbances from the surface or even such ones caused by airborne sources. Since most of the anthropogenic noise contains strong periodic content, whereas aftershock signals do not, the signal-to-noise ratio (SNR) can be increased if periodic signals in the recorded data are suppressed; such signals consist of sines.

In this project an analytic expression for the discrete complex spectrum of a sine, the frequency of which can change with time linearly, has been derived. The expression includes sampling, a limited duration and the Hann window function. With the first derivatives and well-estimated start parameters, the Levenberg-Marquardt algorithm is used to fit the parameters of such a linear-frequency-shift (LFS) sine to single peaks in spectra. The F_{Sum} expression can easily be implemented in typical programming languages. A major disadvantage for applications is the computation effort: on a single core of an Intel i5 processor at $3.1\,\mathrm{GHz}$ the current implementation requires $0.5\,\mu\mathrm{s}$ per fitted value, per sample within the time interval of the spectrum and per iteration step. The processing time for a typical signal is on the order of days per minute of data.

Methods for the evaluation of the fit results are introduced by the systematic analysis of synthetic signals. The fit quality respectively the precision of the fitted parameters increases with decreasing noise to the point where the errors of the fit result are as small as the numerical precision, for example, 10^{-15} relative with double-precision variables. For certain ratios of acceptable false-positive fits to pure Gaussian white noise (GWN), peak-width-dependent thresholds for the application to real data are gained.

In order to test the performance of the fitting procedure, artificial (LFS) sines are added to real signals that are non-periodic. It is demonstrated that sines with arbitrary parameters are fitted and subtracted successfully.

For completely real signals, the performance strongly depends on the data. We played sound files containing (LFS) sines with different parameters during our measurements and recorded the acoustic and seismic signals. Fits of narrow peaks have been very successful both for acoustic and seismic measurements and the processed spectrum is reduced down to the background-noise level. For the monofrequent case the peak magnitude is reduced by at least three orders of magnitude but the reduction factor might be principally unlimited, as indicated for synthetic superpositions. The broadest peak is reduced by 1.5 orders of magnitude only. Here, a slight frequency dependency in the transfer function between played and recorded LFS-sine signals may have led to deviations from the theoretical function for an LFS sine, thus decreasing the fit quality.

For real signals, all peaks which have been fitted successfully are reduced to the level of the background, but typically several smaller and sometimes even stronger peaks remain. Since the ratio of periodic to non-periodic noise is unknown, there is no quantitative measure for the degree of periodic-noise removal. However, one can use the root mean square (RMS) value to find out to what extent a signal is changed during processing.

The acoustic data of a main battle tank have been processed successfully in general. Most of the highest peaks have been subtracted. The strong non-periodic contributions remain in the signal – fitting to the goal of the work. The RMS amplitude of the signal has been reduced by a factor of approximately 3.

Limitations have become visible with certain signals from propeller aircraft and helicopters: the acoustic data of the former contained dominating low-frequency contributions which – in most instances – remained in the signal. The latter seem to contain peaks at very close frequencies leading to superposed peak shapes that do not match the ones of a single (LFS) sine and thus are also not removed.

This work continues the field of research of the working group Physics and Disarmament at the chair Experimentelle Physik III of TU Dortmund. It was started in the 1990s in the frame of the Bochum Verification Project (BVP) to find peaks and series of harmonics in power spectra with the objective of pat-

tern recognition for vehicles [24]. The first step worked on monofrequent sines [16, 25]. For signals of moving vehicles, it turned out that this approach was insufficient to handle cases when the frequency changes within the time used for one spectrum, often by the change of the Doppler shift when the sensor is passed. Thus the next step is a linearly in the time shifting frequency as described in this work. Whether or not it will make sense to advance to higher orders is unknown, but it is doubtful whether it would be of great practical use.

The expression derived and applied in this work is an ideally adjusted filter for arbitrary LFS sines. For synthetic signals it works very precisely and can reproduce signals on a level which is unattainable for notch filters. For all peaks that are not produced by pure (LFS) sines, the fit performance drops, sometimes strongly. The peaks of other real sources are fitted and subtracted mainly successfully.

With regard to the primary motivation of this work, one can state that it is possible to reduce the periodic content of time-series data significantly. However, the signals of the vehicles analysed contain non-periodic components which remain in the signal – but retaining such components for the detection of weak impulsive events has been the goal. The algorithm is developed to a state that it – principally – could be implemented into the standard software used by the inspectors during OSIs, which is developed mainly at the University of Stuttgart in the Institute for Geophysics [26, 27]. If the implementation is done, one will probably not apply the algorithm to all the recorded data in form of a preprocessing procedure because the calculation effort is too intense. Instead the inspectors could pick and process time periods which either have an obvious periodic distortion or contain data that should be improved as much as possible if e.g. an indication exists that interesting signals could be masked – in particular the latter could be desirable if some sensors indicate the presence of an interesting signal whereas others show disturbances.

Obviously, the best conditions to measure small aftershock signals will be achieved if all noise is avoided in advance. The inspected state should be asked to shut down sources of noise and to avoid land and in particular air traffic in the inspection area. Nonetheless, cases could occur in which disturbances will be recorded: on the one hand the inspected state could try to sabotage the OSI; on the other hand the inspectors will produce noise by themselves – by reconnaissance, by flights conducted as part of other measurements (like multi-spectral imaging, air-borne-gamma spectroscopy etc.) and by the maintenance and readout of sensors.

With the described procedure, noise of vehicles can be reduced but not completely removed. It will not allow the detection of smallest aftershock signals next to a busy motorway or the like. Nonetheless, it can increase the SNR, possibly allowing a shorter minimal distance between sensors and potential sources of noise.

In order to solve the problems that have been observed and to optimize and improve the procedure, several directions seem promising for future research:[31]

- Fitting of neighbouring spectral peaks,
- Line tracking over several spectra,
- Simultaneous fit of multiple peaks,
- Searching for harmonics,
- Threshold adjustment for very broad peaks,
- Improvement of start values,
- Reduction of computation effort,
- Possibly also higher orders of frequency shift.

Of these, for early implementation of the procedure the first two seem most important.

In order to implement the algorithm into the existing OSI software the following steps are recommended:

31 For more detail see [14].

- The functionality should be checked with regard to the sample rate used during OSIs which is 500 Hz, much lower than in the example. For the same sources of noise (such as air and land vehicles), similar time intervals should be chosen, meaning a smaller number of data points being processed for each spectrum. This should not reduce the performance of the algorithm; nonetheless it should be analysed.
- During all stages of improvement of the algorithm, functionality should be checked with the data recorded during the "Integrated Field Exercises" of the CTBTO. Additionally, superpositions of real aftershock signals with real (e.g. vehicle) signals should be processed and the result evaluated with regard to the extent of changes to the waveform of the aftershock signal.

Overall, by improving the finding of the hypocenter, this procedure yields a small, but potentially effective contribution to the verification of the Comprehensive Nuclear-Test-Ban Treaty (CTBT) and the deterrence of the conduction of nuclear tests.

Abbreviations

ADC	analogue-digital converter
BVP	Bochum Verification Project
CTBT	Comprehensive Nuclear-Test-Ban Treaty
CTBTO	Comprehensive Nuclear-Test-Ban Treaty Organization – Preparatory Commission
FFT	fast Fourier transform
GWN	Gaussian white noise
IMS	International Monitoring System
LFS	linear frequency shift
MBT	main battle tank
OSI	on-site inspection
RMS	root mean square
SNR	signal-to-noise ratio

Bibliography

[1] National Research Council. *Research required to support comprehensive nuclear test ban treaty monitoring*. National Academy Press, Washington and DC (1997).
URL http://site.ebrary.com/lib/academiccompletetitles/home.action 3

[2] Committee on International Security and Arms Control. Technical issues related to the CTBT. Technical report, Committee on Technical Issues Related to Ratification of the Comprehensive Nuclear Test Ban Treaty, National Academy of Sciences, Policy and Global Affairs (2002). 5

[3] CTBT. http://www.un.org/disarmament/WMD/Nuclear/CTBT.shtml. Accessed: 2014-06-28. 2

[4] CTBT - status of signature and ratification. http://www.ctbto.org/the-treaty/status-of-signature-and-ratification. Accessed: 2014-06-28. 6

[5] armscontrol.org - National Academy of Sciences issued Technical Issues Related to the Comprehensive Nuclear Test Ban Treaty. https://www.armscontrol.org/print/1110. Accessed: 2014-06-29. 7

[6] A. Giuntini, V. Materni, S. Chiappini, R. Carluccio, R. Console, M. Chiappini. Travel-time source specific station correction improves location accuracy. Poster (T1-P61) presented at Science and Technology 2013 Conference, Vienna (2013).
URL http://www.ctbto.org/fileadmin/snt2013/posters/T1-P61.pdf 2

[7] Matjaz Prah, *Overview of CTBT On-Site Inspections*, CTBTO. http://ctbtcourse.files.wordpress.com/2010/10/lecture_13_-ic_osi_matjaz_prah_14102010.pdf. Accessed: 2014-06-29. 2

[8] Zhenfu Li, *On-Site Inspection*, CTBTO. http://www.ctbto.org/fileadmin/user_upload/pdf/ISS_Publication/OSI_41-46.pdf. Accessed: 2014-06-29. 2

[9] CTBTO - Have You Seen a Cavity. http://education.ctbto.org/moodle/pluginfile.php/5605/mod_forum/attachment/476/MELAMUD%20-%20Have%20you%20seen%20a%20cavity.pdf. Accessed: 2014-06-28. 8

[10] A. Belyashov, V. Suvorov, *Studying of upper cross-section of Une area at Semipalatinsk test site according to seismic data (for OSI purposes)*, CTBTO - T3-P116, 2013. http://www.ctbto.org/fileadmin/snt2013/posters/T3-P116.pdf. Accessed: 2014-06-28. 8

[11] M. Liebsch, J. Altmann. *Acoustic-Seismic Coupling in Porous Ground - Measurements and Analysis for OSI Support*. Poster presented at Science And Technology (SNT 2013) Conference, Vienna, 17-21 June (2013). Available from http://www.ctbto.org/fileadmin/snt2013/posters/T3-P7.pdf (1. Sep. 2014). 9, 3

[12] M. Liebsch, J. Altmann. *Acoustic-Seismic Coupling of Broadband Signals - Analysis of Potential Disturbances during CTBT On-Site Inspection Measurements*. Poster presented at European Geosciences Union (EGU 2015) Conference, Vienna, 12-17 April (2015). Available from http://presentations.copernicus.org/EGU2015-696_presentation.pdf (7. Jul. 2015). 9

[13] E. O. Brigham. *The Fast Fourier Transform*. Prentice-Hall, Inc., Englewood Cliffs, NJ, USA (1974). 3, I, 1, 1

[14] F. Gorschlüter. *Sinusoids with linear frequency shift in time series – precise characterisation and removal*. PhD dissertation, Technische Universität Dortmund (2014).
URL https://eldorado.tu-dortmund.de/bitstream/2003/33671/1/Dissertation.pdf 5, 7, I, I, III, 31

[15] J. Altmann. Acoustic Signals of Tracked Vehicles - Evaluations in the Spectral and Time Domain for Co-operative Verification of Disarmament and Peace-keeping Agreements (unpublished). Technical report, Ruhr-Universität Bochum (1999). 5, 25

[16] F. Gorschlüter. *Messung, Erkennung und Unterdrückung periodischer akustischer und seismischer Störsignale*. Diploma thesis, Technische Universität Dortmund (2009). 5, 5

[17] W. H. Press, S. A. Teukolsky, W. T. Vetterling, B. P. Flannery. *Numerical recipes in Pascal: the art of scientific computing*. Cambridge University Press, 1st edition (1989). I

[18] E. O. Brigham. *The Fast Fourier Transform and Its Applications*. Prentice-Hall, Inc., Upper Saddle River, NJ, USA (1988). I, 5

[19] Y. Katznelson. *An Introduction to Harmonic Analysis*. Dover Publications Inc., New York (1976).
URL http://opac.inria.fr/record=b1077889 7

[20] M. Bischoff, A. Cete, R. Fritschen, T. Meier. Coal mining induced seismicity in the Ruhr Area, Germany. *Pure Appl. Geophys.* **167**, 63 (2010). II

[21] F. Gorschlüter, J. Altmann. *Subtraction of Periodic Disturbances in Seismic Aftershock Recordings*. Poster presented at Science and Technology (SnT2013) Conference, Vienna, 17-21 June (2013). Available from http://www.ctbto.org/fileadmin/snt2013/posters/T3-P103.pdf (17. Sep. 2014). 13

[22] H. Militzer, F. Weber. *Angewandte Geophysik Bd. 3*. Akademie-Verlag Berlin (1987). 20, 21

[23] J. Altmann. Acoustic and Seismic Signals of Heavy Military Vehicles for Co-operative Verification. *Journal of Sound and Vibration* **273**, 713 (2004). II, 24, 25

[24] J. Altmann, S. Linev, A. Weiss. Acoustic-seismic detection and classification of military vehicles – developing tools for disarmament and peace-keeping. *Applied Acoustics* **63**(10), 1085 (2002). doi:10.1016/S0003-682X(02)00021-X. 24, 5

[25] F. Gorschlüter, J. Altmann. Suppression of periodic disturbances in seismic aftershock recordings for better localisation of underground explosions. *Pure and Applied Geophysics* **171**(3-5), 561 (2014). doi:10.1007/s00024-012-0617-y. 5

[26] M. Joswig. Nanoseismic monitoring fills the gap between microseismic networks and passive seismic. *First Break* **26**(10), 117 (2008). 5

[27] NanoseismicSuite - nanoseismic monitoring. http://nano.geophys.uni-stuttgart.de/. Accessed: 2015-07-07. 5

About the author

Dr. rer. nat. Felix Gorschlüter studied physics at the Technische Universität Dortmund. Since 2007 he was a member of the working group Physics and Disarmament at the Chair Experimentelle Physik III. He wrote his Diploma thesis (2009) about the reducibility of periodic noise from time-series (constant-frequency) data to support on-site inspections of the CTBTO. In his doctoral work (thesis 2014) he continued the research, expanded to frequencies changing linearly with time and improved the algorithms to a point where implementation can start.

Folgende Publikationen (Auswahl) sind über die DSF zu beziehen:

Forschung DSF:

- Jürgen Rüland/Maria-Gabriela Manea: How much an Actor and under which Logics of Action? Roles of Parliaments in the Establishment of Democratic Control of the Armed Forces in Indonesia and Nigeria. Osnabrück 2012 (Heft 34).
- Ulrich Schneckener: Zwischen Vermittlung und Normdiffusion. Möglichkeiten und Grenzen internationaler NGOs im Umgang mit nicht-staatlichen Gewaltakteuren. Osnabrück 2013 (Heft 35).
- Martina Fischer/Ljubinka Petrović-Ziemer: Dealing with the Past and Peacebuilding in the Western Balkans. Osnabrück 2015 (Heft 36).
- Oliver Meier/Iris Hunger: Between Control and Cooperation: Dual-Use, Technology Transfers and the Non-Proliferation of Weapons of Mass Destruction. Osnabrück 2014 (Heft 37).
- Bettina Engels/Sven Chojnacki: Umweltwandel, Ernährungskrisen und Konflikt. Räumliche soziale und politische Dynamiken. Osnabrück 2015 (Heft 38).
- Philipp Stroh: Humanitär-völkerrechtliche Rahmenbedingungen für den Einsatz luftgestützter unbemannter militärischer Kampfsysteme im bewaffneten Konflikt. Osnabrück 2016 (Heft 40).

Arbeitspapiere DSF:

- Interventionen zum Schutz der Zivilbevölkerung? Herausforderungen und Dilemmata in Zeiten der Responsibility to Protect (RtoP). Beiträge zum Parlamentarischen Abend der DSF am 20. September 2011 in Berlin. Osnabrück 2012 (Heft 8).

Forum DSF:

- Präsentation und öffentliche Übergabe des Sonderpostwertzeichens „Nie wieder Krieg" 1914 – Ausbruch Erster Weltkrieg am 29. August 2014 im Friedenssaal des historischen Rathauses der Stadt Osnabrück. Osnabrück 2015 (Heft 5).

Jahresberichte DSF:

- Jahresberichte 2001-2012.

Publikationen aus eigenen Tagungen und Kooperationsveranstaltungen:

- Roland Czada/Thomas Held/Markus Weingardt (Eds): Religions and World Peace. Religious Capacities for Conflict Resolution and Peacebuilding (= Religion – Konflikt – Frieden, Bd. 5) Baden-Baden: Nomos 2012.
- Reinhold Mokrosch/Roland Czada/Thomas Held (Hrsg.): Religionen und Weltfrieden. Friedens- und Konfliktlösungspotenzial von Religionsgemeinschaften. Stuttgart: Kohlhammer 2013.
- Tobias Debiel/Thomas Held/Ulrich Schneckener (Eds): Peacebuilding in Crisis. Rethinking paradigms and practices of transnational cooperation. London/New York: Routledge 2016.